11-18-2020

An Investigative Study of Combustion and Emissions with Noise and Vibrations Of Synthetic Fuels within an Aero-Gas Turbine

Camille J. Phillips
Georgia Southern University

An Investigative Study of Combustion and Emissions with Noise and Vibrations Of Synthetic Fuels within an Aero-Gas Turbine

An Honors Thesis submitted in partial fulfillment of the requirements for Honors in Mechanical Engineering.

By Camille Phillips
Under the mentorship of Dr. Valentin Soloiu

Abstract

The pollution from the aerospace transportation is rapidly becoming the largest source of greenhouse gas (GHG) emissions. The FAA expects aviation emissions to almost triple by 2050, making the aerospace industry responsible for the release of approximately 25% of the global carbon dioxide budget. These aviation emissions, including CO_2 and NO_x, as well as other GHGs, contribute to the destruction of ozone layer. Carbon dioxide emissions have a particularly negative effect on humans, leading to airway diseases especially in children and elderly. To combat the addition of further GHG emissions into the atmosphere, it is necessary to minimize the usage of fossil fuels and explore alternatives. Fischer-Tropsch synthetic fuels can be produced from recycled biomass and have high potential for both commercial and military use due to their favorable balance of fuel properties. The purpose of this study is to analyze synthetic kerosene fuel IPK through experimentation in a turbojet engine. The combustion, emissions, noise, and vibrations characteristics of the synthetic kerosene fuel will be investigated and compared to those of standard jet fuel (Jet A). Electronic data acquisition systems, including microphones, accelerometers, load cells, and a state of art emissions analyzer will be employed to test the turbojet.

Thesis Mentor:_____

Dr. Valentin Soloiu

Honors Director:_____

Dr. Steven Engel

November 2020
Department of Mechanical Engineering
University Honors Program
Georgia Southern University

Acknowledgements

I would like to thank my faculty advisor Dr. Valentin Soloiu for the immense amount of time he commits to teaching me and the other student researchers in his lab. I am very thankful for his mentorship and continuous support especially amidst and following the pandemic. I would also like to thank all of the lab members who have helped me to complete experimental trials, especially Margaret Kilpatrick, Tyler Wiley, Cesar Carapia, Aliyah Knowles, David Mothershed, Levi Mckinney, Richard Smith, Amanda Weaver, Drake Grall, David Obando, and Austin Brant. Thank you for your commitment to helping me, for all of our lively discussions, and for your continued encouragement throughout my time doing research.

I would like to thank the Department of Mechanical Engineering for their support, guidance, and knowledge that they have provided me during my time here at Georgia Southern. I would like to thank the University Honors Program and faculty for pushing me to succeed during my time here at Georgia Southern.

Finally, I would like to thank my friends and family for their constant support and encouragement of me and my dreams.

This research was supported by DoD-NSF Assure REU Site Award: 1950207 and experimental fuel contributions from the Air Force Research Laboratory.

Table of Contents

List of Figures

List of Tables

1 Introduction

The objective of this study was to investigate synthetic kerosene combustion and its effects on noise, vibrations and gaseous emissions in an aero-gas turbine. Iso-Parrafinic Kerosene (IPK) and Jet A were tested to better understand the properties of the fuels.

1.1 Fuel Analysis

Jet fuel is composed of hydrocarbon chains that can vary based on the source and manufacturing processes. The sources for jet fuel include crude oil, natural gas liquid condensates, heavy oil, shale oil, and oil sands, as well as qualifying additives. There are stringent requirements for all jet fuels in commercial and international aviation as well as those used in military and aerospace aviation. Fuels that contain synthetic components derived from non-petroleum sources are strictly regulated, with the type, amount, and quality of additives being closely controlled.

The standard jet fuels used in the United States are Jet A and JP-8. As reduction in emissions is becoming a widespread goal in the aircraft industry, alternatives to jet fuels could potentially reduce the pollutants produced during combustion due to their base feedstock and production process (James I. Hileman, 2009). Possible alternatives to the standard fuels are synthetic fuels derived from coal and natural gas using the Fischer-Tropsch process. This method converts raw carbon sources such as coal, natural gas, biomass, or organic waste into synthesis gas (syngas) before indirectly liquefying them into hydrocarbons (Klerk, 2000). Following the liquefication of the syngas, a synthetic crude oil is produced and refined into fuels and various petroleum chemicals (Klerk, 2000). Some Fischer-Tropsch fuels are certified for commercial use as blends with standard fuels and more fuels are under development using this method (Tara J Fortin, 2015).

In this study, a Fischer-Tropsch synthetic fuel, will be tested and compared to known data. The testing will include an investigation of the emissions characteristics of of a synthetic fuel and Jet A, the standard jet fuel. The synthetic fuel, Sasol Iso-paraffinic Kerosene (IPK), has been tested prior to this study and will be re-examined to determine the repeatability of the experimental results. Sasol IPK is a coal derived kerosene made up of iso-paraffins, hydrocarbons arranged in straight or branched chains (Moses 2008). Table 1 shows and compares the ASTM standards and fuel properties of Jet A and Sasol IPK (Chi Zhang, 2014).

Table 1. ASTM Standard and Properties of Conventional and Alternative Jet Fuels (Chi Zhang, 2014)

Property	ASTM Standard	Jet A	Sasol IPK
POSF number	--	4658	5642
Composition			
n – Paraffins (wt%)	--	28	2.1
Iso – Paraffins (wt%)	--	29	88
Cyclo – Paraffins (wt%)	--	20	9
Aromatics (wt%)	Report	20	<0.5
Total Sulfur (wt%)	Max 0.3	--	<0.001
Distillation			
Initial boiling point (°C)	Report	158	149
10% recovered (°C)	Max 205	184	166
20% recovered (°C)	Report	192	170
50% recovered (°C)	Report	213	180
90% recovered (°C)	Report	248	208
Final boiling point (°C)	Max. 300	269	228
Flash point (°C)	Min. 38	47	44
Freezing point (°C)	Max. -47	- 49	< -78
Density @ 15 °C (kg/m^3)	665-840	806	762
Viscosity @ -20 °C (cSt)	Max. 8.0	5.2	3.6
Neat heat of combustion (MJ/kg)	Min. 42.8	42.8	44
Smoke point (mm)	Min 19.0	21	> 40
H/C molar ratio	--	1.957	2.119
Molecular weight (g/mol)	--	142	156

ASTM standards require alternative jet fuels to have a heat of combustion greater than 42.8 MJ/kg, a flash point greater than 38 °C, and a freezing point higher than -47 °C (Moses, 2008). Because alternative jet fuels have lower amounts of cyclo-paraffins and aromatics than standard jet fuels, their density values fall short of the minimum ASTM requirement of 775 kg/m〖^3〗 at 15 °C (Moses, 2008). For this reason, options are limited for blending alternative fuels with standard fuels.

1.2 Emissions

Greenhouse gases are produced primarily through the burning of fossil fuels for electricity, heat, agricultural or manufacturing processes, and transportation. When these sources release greenhouse gases into the atmosphere, the gases absorb and radiate heat from sunlight, causing the Earth's temperature to rise. Due to increases in greenhouse gas production in the last century, it has been observed that the Earth's climate is changing at an alarming rate. According to the National Climate Assessment (Program, Observed Change | National Climate Assessment, n.d.) climactic effects from greenhouse gases include increased temperatures at the Earth's surface, troposphere, and oceans, a decrease in snow and ice over the poles due to melting, and growing season lengths. The United States Environmental Protection Agency attribute changes in weather patterns and extreme weather events, rising seas levels, and higher acidity levels in oceans to climate change as well (EPA, 2016).

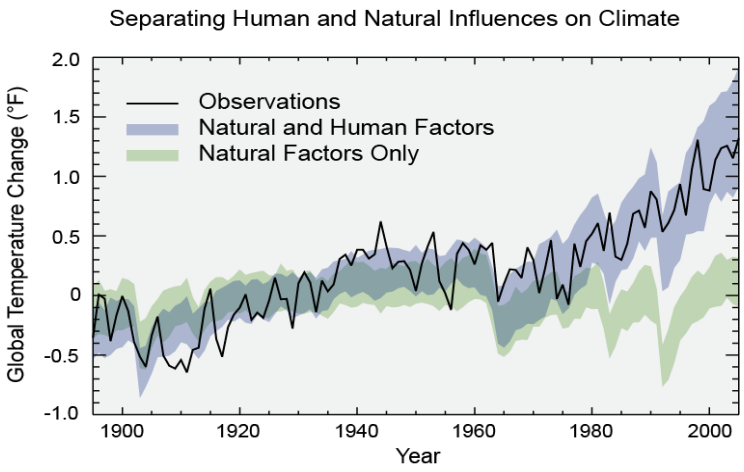

Figure 1. Human and Natural Influences on Climate Change (Program, Observed Change | National Climate Assessment, n.d.)

The fossil fuel emissions from aviation include carbon dioxide (CO_2), methane (CH_4), nitrous oxide (NOx), and black carbon (soot). Because the bulk of aircraft emissions are produced at cruising altitudes, they have a greater negative effect than greenhouse gases released at the Earth's surface. Figure 1 above displays the observed global averages in temperature (Program, Observed Change | National Climate Assessment, n.d.) Global warming effects can only be explained by the greenhouse gas production from humans as seen from the diversion of the black observation trendline from following the natural factors trend to following the human induced and natural factors trend.

Similarly, Figure 2 depicts how the global annual average temperature has increased by more than 1.5° since 1880. The red bars show the temperatures above the long-term average, and the blue bars display temperatures below the long-term average. The black line is the atmospheric carbon dioxide (CO_2) concentration in parts per million (ppm). It is seen in the figure that there is a clear long-term global warming trend, but the relative year to year trend fluctuates from increasing to decreasing.

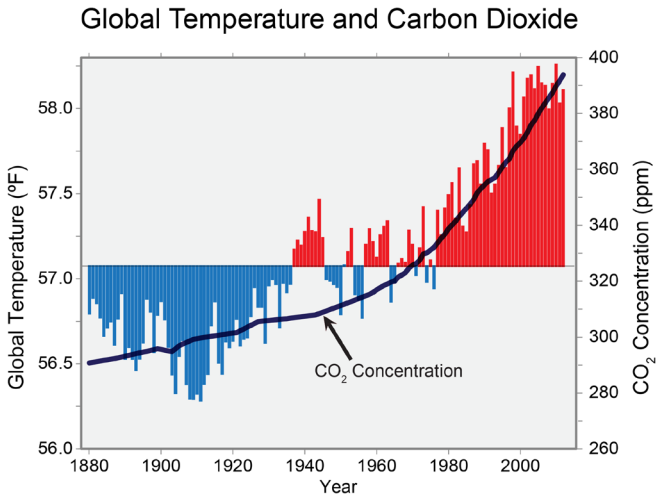

Figure 2. Global Temperature and Carbon Dioxide from 1880 to the early 2000s (Program, Observed Change | National Climate Assessment, n.d.)

According to the International Council on Clean Transportation (ICCT) (Brandon Graver, Zhang, & Dan Rutherford, 2018), the aircraft industry is rapidly becoming a leading producer of greenhouse gases, as aviation emissions are expected to account for almost 25% of the global carbon budget within the next thirty years. This is in part because air transportation continues to be the primary mode of international transportation. However, because aircraft emissions are produced at cruising altitudes, high in the atmosphere, they have a greater negative effect than greenhouse gases released at the Earth's surface. Figure 3 displays how at cruising altitude, carbon dioxide, nitrogen oxides, water vapor, sulphates, and soot are released from jet engines (Fleming, 2009). For every gallon of jet fuel burned, approximately 21 pounds of carbon dioxide are emitted (Fleming, 2009).

Carbon dioxide emissions in particular are a direct result of fuel burn, with 21 pounds of carbon dioxide emitted for every gallon of jet fuel burned (Fleming, 2009). When water vapor released from a jet engine condenses at certain temperatures at higher altitudes, contrails are often produced (Fleming, 2009). Contrails are white, cloudlike trails

that often can be seen following a jet. Contrails stay in the sky for hours, spreading thin before disappearing, and can trap heat that would otherwise dissipate, contributing to global warming. Contrails also are believed to contribute to the formation of cirrus clouds, similarly thought to have a warming effect on the earth's atmosphere (Fleming, 2009).

The Federal Aviation Administration forecasts that fuel consumption of U.S.-based airlines will increase an average of 1.6 percent per year before 2025 (Fleming, 2009). Due to this expected increase in fuel consumption, the aircraft industry is looking for ways to improve fuel efficiencies and mitigate greenhouse gas emissions (Tara J Fortin, 2015). In 2009, the International Air Transport Association decided to target an improvement in fuel efficiency by an average of 1.5% per year through 2020, as well as a reduction in carbon dioxide emissions by 50% relative to 2005 levels by the year 2050 (Tara J Fortin, 2015). To aid in reaching this goal, it is necessary to explore alternative jet fuels.

1.3 Noise and Vibrations

Principles of Sound

A sound wave is a vibrational disturbance in a medium, usually air, that carries energy from one place to another without there being any contact between the two places. The production of a sound wave is caused by the vibrations of the particular medium through which it passes. A sound wave is sinusoidal and can be described in terms of wavelength, period, and amplitude. The length of one complete wave, or the minimum distance in which a sound wave repeats itself, is called wavelength. The equation for wavelength is given in Equation 1 below (Measuring Sound, 1984).

$$Wavelength\ (\lambda) = \frac{speed\ of\ sound\ (\frac{m}{s})}{frequency\ (Hz)} \quad (1)$$

The amplitude of a wave is equal to the maximum displacement of the particles of the medium from their original positions and corresponds to the volume of sound produced.

On a wavelength graph, the amplitude is the height of the wave from the wave center (typically from the center axis). The period of a sound wave is the time required to produce one complete wave. Period and frequency are inverses of each other, as the number of complete waves produced in one second it called the frequency of the sound wave. The characteristics of sound waves are shown below in Figure 4 and will be discussed further in a later section of this study.

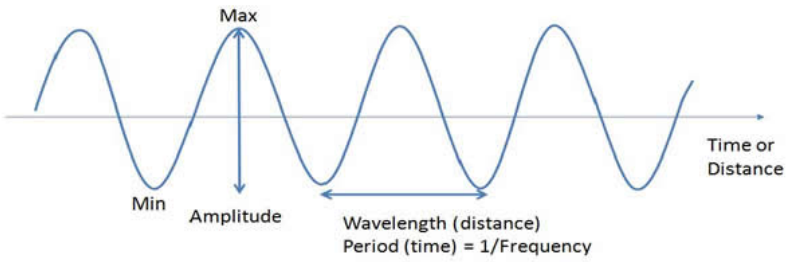

Figure 3. Characteristics of a Sound Wave (Atif Qasim MD, n.d.)

Sound measurement allows for the analysis of unpleasant sounds to the human ear as well as understanding which sounds are potentially harmful to humans. Sound can be described in terms of amplitude of sound pressure fluctuations. The unit of sound pressure or volume of a sound is measured in Pascals (Pa), with the quietest sound a human can hear corresponding to 20 µPa (micro-pascals). To promote the usage of reasonably units of measurement, the decibel (dB) scale is used to measure sound pressure. The decibel is a ratio between a measured quantity and an agreed reference level. The decibel scale is logarithmic and uses the hearing threshold of 20 µPa as a reference level correlating to 0 dB. Because the decibel scale is logarithmic, it is able to compress a range of Pa unit sound measurements into a range of about 20 dB and gives a better approximation of the loudness of sounds to humans. The sound pressure level (SPL) formula for measurements in dB is

given in Equation 2 below with p corresponding to the sound pressure in Pa and p_o signifying the reference sound pressure level in Pa.

$$SPL\ (dB) = 10log_{10}(\frac{p^2}{p_o^2}) \quad (2)$$

Aircraft Noise

As air traffic continues to increase, noise caused by aircraft operations in the surrounding areas of airports is becoming a more prevalent issue, both environmentally and technologically, in today's society (Mofid Gorii-Bandpy, 2012). According to the Impacts of Science Group of the Committee for Aviation Environmental Protection of the International Civil Aviation Organization, noise or "unwanted sound" from aircrafts causes community annoyance, disrupts sleep patterns, has negative effects on the academic performance of children, and has the potential to increase the risk of cardiovascular disease for people who live in the close vicinity of airports (Mathias Basner). Many of the health problems attributed to aviation related noise stem from sleep disruption or deprivation (Swift, 2010). Both sleep disruption and deprivation arouse the sympathetic nervous system, which can change the balance of the body's hunger regulating hormones, leading to weight loss or weight gain (Swift, 2010). Being severely overweight is a risk factor for cardiovascular and metabolic diseases. Similarly, sleep disruption can disrupt normal glucose management and impair the nocturnal reduction in blood pressure, potentially leading to hypertension, heart disease, and diabetes (Swift, 2010). Figure 4 displays the potential pathways for the health effects of noise through sleep disturbance.

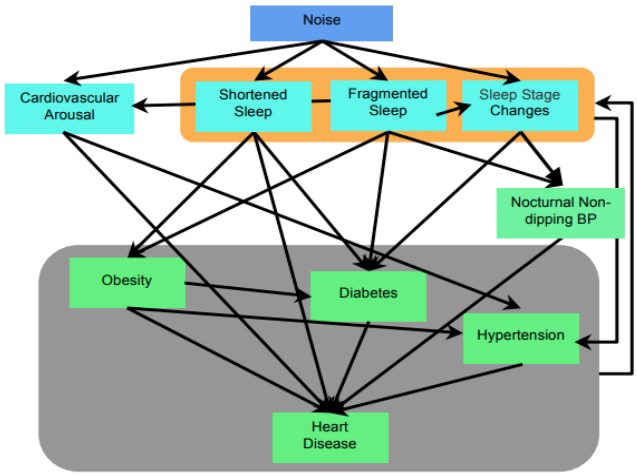

Figure 4. Proposed Potential Pathways for the Health Effects of Noise Through Sleep Disturbance (Swift, 2010)

The FAA strives to control aircraft noise through measures such as noise reduction at the source (development and adoption of quieter aircraft), soundproofing and buyouts of buildings near airports, operational flight control measures, and land use planning strategies (Transporation, 2018). In an effort to contribute to noise reduction at the source, this study analyzes the noise and vibrations produced when different synthetic fuel types are burned within a turbojet engine compared to the standard fuel, Jet A. Vibration is defined as the oscillating, reciprocating, or other type of period motion of a rigid or elastic body forced from a position or state of equilibrium (David Carbaugh, n.d.). Vibration and noise are closely related in that noise is a type of vibration that excites the air so much that it can be heard (David Carbaugh, n.d.). For this reason, while societal discontent has called attention to the issue of aircraft noise, the vibration of aircraft must be examined alongside the noise of an aircraft to work towards a solution.

Principles of Vibration

Vibration is defined as oscillation that occurs about an equilibrium point, or any mechanical motion that repeats itself after an interval of time (Rao, 2010). Of the many

classifications of vibrations, only a few types will be discussed. Free vibration is when, after an initial disturbance, an object or system is left to vibrate freely with no obstacles stopping the periodic motion (Rao, 2010). In contrast, forced vibration is when a system is subjected to an external force after the initial disturbance (Rao, 2010). Forced vibration occurs in engines and must be monitored to avoid resonance – a situation in which the system undergoes extremely large and hazardous oscillations (Rao, 2010). Resonance causes failures in a variety of structures, to include buildings, bridges, turbines, and airplanes. In the case of vibration in which there is no net loss of energy through resistance in oscillation or friction, the vibration is defined as undamped (Rao, 2010). Damping vibration is when any energy is lost due to the vibration occurring. The damping effect for many systems can be negligible and is often disregarded in vibrations analysis.

Aircraft Noise and Vibrations

Every airplane experiences a unique set of normal vibrational patterns during operation due to mass distribution and structural stiffness at certain frequencies (David Carbaugh, n.d.). Airflow over different surfaces on a plane results in low level vibrations, which is usually recognized as background noise. Vibrations are more significant and visible, yet still normal, when an airplane experiences turbulent air or when a spool imbalance excites the engine. The spool is a shaft on which the turbines of a jet engine rotates.

Aircraft noise is generated from various sections within an aircraft engine, to include the air frame, propeller, compressor, turbine, combustor, and jet exhaust (Kilpatrick, 2019). A large amount of noise comes from the air frame during take-off and landing, due to the turbulent, separated flow around different parts of the landing gear

(Mathias Basner). Figure 5 below describes the main areas of noise on an aircraft. The darkest regions on the airframe signify the origins of the highest levels of noise. In reference to noise produced from the turbine, the majority of the noise comes from the fan sections, as can be seen from Figure 6 (M Dost, 2016).

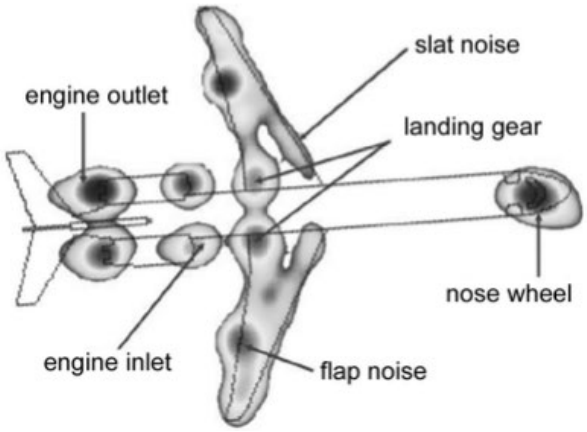

Figure 5. Airframe Noise Sources (Mathias Basner)

The landing gear has various cavities and sharp edges, making the flow-field complex and causing broadband noise, or noise that is distributed over a wide section of audible range (Mathias Basner). Air frame noise is also produced from air flowing over and around the aircraft during flight, and when turbulent flow occurs along the wing slats when the landing gear is deployed (Mathias Basner). The leading-edge slat and trailing edge slat regions have been found to be the sources of high tonal noise, or noises that occur at a single frequency, and this tonal noise significantly increase the perceived noise level (Mathias Basner). The darkest regions on the airframe signify the origins of the highest levels of noise. In reference to noise produced from the turbine, the majority of the noise comes from the fan sections, as can be seen from Figure 6 (M Dost, 2016).

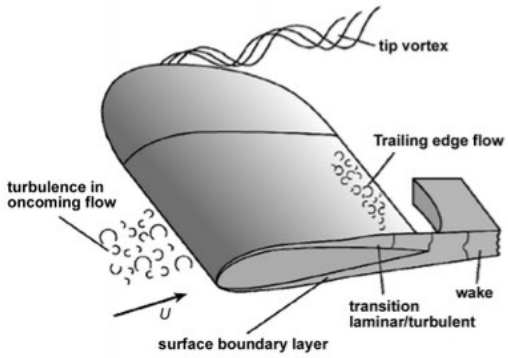

Figure 6. Wing Noise Sources (Mathias Basner)

Noise stems from the turbine and compressor, and jet exhaust as well, and their respective magnitudes and directions of the noise also displayed. The powerful mixing of the turbulent exhaust gases and atmosphere cause the jet exhaust noise (Purdue University 1998). Because there is a significant difference in speed between the jet exhaust and the atmosphere, there is an intense shearing that also causes substantial noise (Purdue University 1998). The highest frequency noise emanates from the small eddies nearest to the outlet exhaust, with the turbulence of the larger eddies causing lower frequencies further downstream (Purdue University 1998). A shock wave is also produced when the exhaust exceeds the speed of sound (Purdue University 1998). However, if the exhaust velocity is reduced to better match the velocity of the atmosphere, the noise level of the jet exhaust can be similarly reduced (Purdue University 1998).

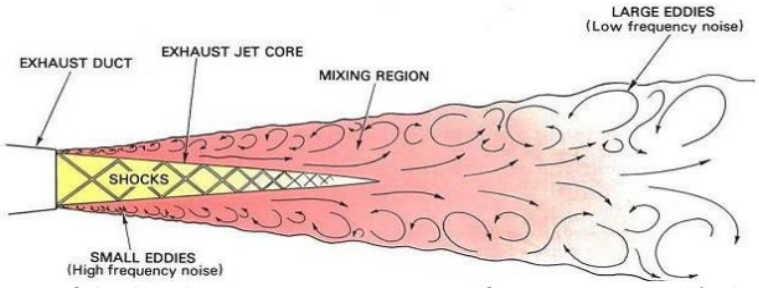

Figure 7. Origin of Shock and Mixing Noise Components of Jet Noise Spectrum (M Dost, 2016)

2 Literature Review

2.1 Fuel Properties

According to (Tara J Fortin, 2015), the primary types of jet fuel used in the United States are Jet A, Jet A-1 which contains a dissipater additive, and JP-8 (Tara J Fortin, 2015). Created during World War II, Fischer Tropsch synthesis offers liquid hydrocarbon fuels as an alternative to coal gasification. This method converts raw carbon sources such as coal, natural gas, biomass, or organic waste into synthesis gas before indirectly liquefying them into hydrocarbons and refining them into fuels (Tara J Fortin, 2015). To quickly summarize the process, the input carbon source is gasified to form a synthesis gas composed of carbon monoxide and hydrogen. This syngas is converted into primary products of wax, hydrocarbon condensate, tail gas, and reaction water. The wax is chemically split into hydrocarbon liquids parts that are, by molecular weight, smaller. Meanwhile, surplus hydrogen from the tail gas and feed syngas stream is extracted using a recovery unit. These reaction products are portioned into diesel and jet fuel.

Fischer Tropsch fuels are classified based on the source of the synthesis gas; when a liquid fuel is synthesized from coal, it is called a coal-to-liquid (CTL). Similarly, when a liquid fuel is synthesized from gas, it is called a gas-to-liquid (GTL). The compositions of the FT fuels are dependent upon the crude carbon source from which the fuel was derived as well as the specific refining process implemented (Tara J Fortin, 2015). Some FT fuels from the hydrotreated renewable jet fuel (HRJ fuel) category are certified for commercial use as blends with the previously mentioned standard jet fuels (Tara J Fortin, 2015). There are stringent federal requirements to become a qualified blending agent with the acceptable conventional fuels.

In a study by Julia Heimberger and Martin Muinos (Julia Heimberger), aviation fuel composition has four molecular classes: paraffins (alkenes), olefins, napthenes, and aromatics. Paraffinic fuels are also known as kerosene or clean diesel fuels that are made through the Fischer Tropsch process from natural gas, biomass, or vegetable oils and animal fats. Olefinic fuel is produced from olefinic hydrocarbons, which are unsaturated hydrocarbon compounds that contain at least one carbon to carbon double bond. Olefinic fuel, created through man made compounds of oil and natural gas, is produced from crude oil refineries and chemical plants. Napthenes, also known as cycloparaffins, have the same chemical formula as olefins but are paraffins that are bent into a ring shape (Sadeghbeigi, 2012). The high-performance gasoline that is derived from napthenes has more aromatics and is heavier than gasoline produced from cracking paraffins. Aromatics are base components of gasoline that are derived from crude oil. Aromatics can be manipulated into chemical substances in mixtures to increase fuel performance.

In reference to the ASTM Standard and Properties of Conventional and Alternative Jet Fuels (Chi Zhang, 2014), by weight percentage, Jet A is composed of more n-paraffins, cyclo paraffins and aromatics. As the name implies, the FT fuel (IPK) is composed of mostly iso-paraffins by weight percentage but also leads in sulfur weight percentage against Jet A. In a later section, the emissions of both fuels as a result of their compositions will be discussed.

Prominent fuel properties that effect combustion behavior include hydrogen to carbon molar ratio (H/C), molecular weight (MW), derived cetane number (DCN), and threshold sooting index (TSI). In the past century, fuel usage has trended towards higher hydrogen to carbon molar ratios because as the hydrogen to carbon ratio increases, energy

efficiency increases and CO2 emissions decrease (Balachandar Gopalakrishnan, 2019). In recent years, natural gas has been found to lower carbon content in comparison to oil. Additionally, the carbon content is even lower in biofuels, with biofuels like hydrogen having a zero carbon to hydrogen ratio. A helpful determinator of efficiency and emissions characteristics of fuels is the H/C ratio, and therefore it will be considered in this study. In a study concerning the fuel properties during blending of iso-paraffinic kerosene and jet fuel performed by (Richard Striebich, 2008), as FT fuel is added to standard jet fuels (creating an FT blended fuel), the blends show increased hydrogen content, thereby improving the H/C ratio.

The molecular weight (MW) of a fuel is defined as the ratio of the average mass of one molecule of a fuel to one twelfth the mass of a carbon-12 atom. In the same study by (Richard Striebich, 2008), a linear dependence of the flash point of the fuel on percentage of FT blend was found. It was determined that the dependence between flash point and percentage of FT fuel was because the volatility and molecular weight were similar to standard aviation fuels.

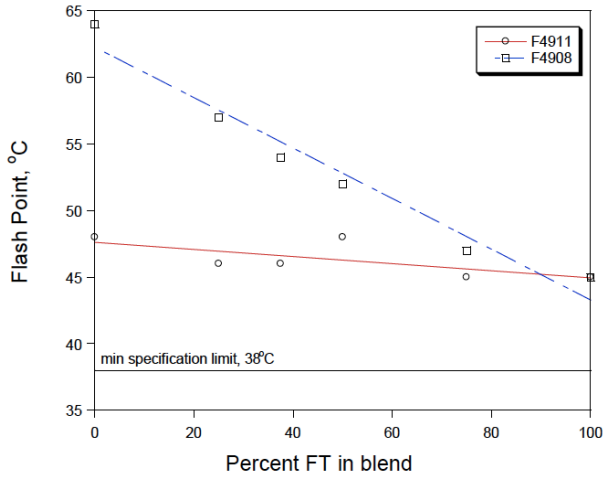

Figure 8. Dependence of flash point (ASTM D93) on blend percentage of FT-derived fuel (Richard Striebich, 2008)

A fuel's cetane number is a relative measure of the time delay between the injection of fuel into the chamber and start of combustion (J. Yanowitz, 2017). A derived cetane number is largely based on fuel ignition delay (using a constant volume combustion chamber) and therefore is the measurement that will be used for analysis. Ignition delay is the time lag between the start of fuel injection and the start of combustion when the air fuel mixture ignites. As ignition delay increases, the premixing of fuel and air also increases which reduces the duration of combustion. This causes more fuel to remain unburnt, decreasing the efficiency of the combustion process. A short ignition delay allows for an increase in pressure before combustion and allows more of the premixed air and fuel to burn, increasing the efficiency of the combustion process. When examining jet fuels and how they combust, ignition delay is a primary factor in determining the efficiency of the fuels.

According to (Sylvester Abanteriba, 2016), ignition delay is dependent on fuel volatility, which is tied to the composition and structure of the fuel. In combination with findings from (R., 2012), longer ignition delay times from iso-paraffins and aromatics were credited to the higher stability of the molecular structure that needs high activation energies to spark the combustion process. Similarly, (Ghosh P., 2006) found that generally speaking, fuels with high concentrations of n-paraffins have low ignition delay times. When examining the fuel compositions of Jet A and IPK, Jet A contains a higher percentage by weight of n-paraffins over IPK. Along with IPK's high iso-paraffin content, it can be assumed that IPK has a higher ignition delay time than Jet A leading to a lower efficiency of IPK fuel burn.

A threshold sooting index (TSI) is a ranking system for the sooting tendency of fuels. When a combustion cycle is incomplete due to reduced supplies of oxygen and lower than ideal temperatures, soot is produced which is made primarily of black carbon. (Yi Yang, 2007) found that TSI performs the best for predicting soot formation in turbine combustion against other parameters like hydrogen content and smoke point that are often implemented for predictive measurements of soot formation. From (Robert J. Santoro, 2007), it was found that the threshold sooting index for diffusion flames is a sum of a constant a times the ratio of molecular weight to smoke point and a second constant b . Both constants are dependent on the apparatus for smoke point measurement. According to (Yi Yang, 2007), the TSI has a linear correlation with the ratio of fuel MW and smoke point in a diffusion flame. A high smoke point means that a fuel has a low smoke producing tendency. Generally speaking, the more aromatics a fuel contains, the more smoke it produces, meaning that it has a lower smoke point. From all of this information, an ideal combination for a fuel to have a low TSI (producing a low amount of soot) would be a low molecular weight and a very high smoke point. This combination would make the ratio very small, producing a low TSI. According to Figure 4, Jet A has a MW/ smoke point ratio of $\frac{21}{142} = 0.14789$ while IPK has a ratio of $\frac{40}{156} = 0.25641$. Because Jet A has a lower ratio, it can be assumed that Jet A will have a lower soot production that IPK.

Other important properties of jet fuels and their potential alternatives, as considered by (Tara J Fortin, 2015), include thermo-physical properties such as viscosity lower heating value (LHV), density, and thermal stability (TGA/DTA). Viscosity is an important element in fuel combustion and is closely tied to fuel efficiency. Viscosity is the property of internal resistance against flow. If a fuel has a high viscosity, the fuel pump can be damaged during

the cycle process due to high pressure or could cause improper injection of the fuel, leading to combustion inefficiency. If a fuel has a low viscosity, too much fuel will be injected into the combustion chamber and can cause incomplete combustion with a high amount of negative emissions as a result. Viscosity also influences how fast the fuel is injected and how the fuel atomizes, as well as the droplet velocity during injection.

The LHV of a fuel is the amount of heat released during combustion. The LHV is important in determining what the specific output power of the fuel combustion will be. TGA/ DTA (Thermogravimetric analysis / differential thermal analysis) are evaluations of chemical reactions that provide properties of fuels such as enthalpy, thermal capacity, mass changes, and the coefficient of heat expansion (Simons, 2016). TGA specifically measures changes in weight of a fuel in relation to changes in temperature of a fuel during combustion. A measured weight loss curve is obtained through this analysis and the derivative of that weight loss curve can be used to define at which point the weight loss is most apparent. This allows for the determination of the thermal stability of a fuel. DTA studies the material or fuel in question and uses an inert reference material. Both undergo identical thermal cycles and differences in temperature between the studied fuel and the reference sample are found. In a DTA, the change in temperature between the specific fuel and the reference sample is plotted against time or temperature and can show the changes in heat and temperature.

The fuel properties analyzed in this study were viscosity, LHV, TGA/DTA, cetane number (including NTC, LTHR, and AHRR) and their combustion characteristics that were evaluated using a constant volume combustion chamber (CVCC).

2.2 Gaseous Emissions

In the above section, the components of Jet A and IPK fuel were discussed because the fuel content can have a large impact how the fuel combusts. By extension, the nature of the fuel combustion can affect the quantity and type of emissions that fuel burn releases.

Emissions from jet fuel combustion processes include carbon dioxide, water vapor, nitrous oxides, hydrocarbons, volatile organic compounds, carbon monoxide, sulfur oxides, and particulates (Aviation & Emissions A Primer, 2005). Carbon dioxide is the largest emissions species, accounting for 70% of the jet fuel exhaust. When fuel combines with oxygen in the air during a complete combustion cycle, carbon dioxide is released and mixes with atmospheric gases. These mixtures of carbon dioxide have a direct warming effect on the earth and their long life-cycles cause them to be especially detrimental to the environment. As hydrogen in the fuel combines with oxygen in the air, water vapor is released into the atmosphere. Jet exhaust is made up of approximately 30% water vapor. The water vapor freezes when it reaches the cold outside air temperature, causing contrails and later cirrus clouds which trap infrared rays. Even with their short life span, these trapped rays have a warming effect that is greater than the effect of all carbon dioxide emissions combined.

When incomplete combustion of jet fuels occurs, hydrocarbons and carbon monoxide particulates form. Particulates are atmospheric aerosol particles that are microscopic in size; particulate matter can be solid or liquid and their microscopic size allows them to be suspended in the air for extended periods of time (Mohamad P. Zakaria, 2018).

Ultra-fine particles (UFPS) and polycyclic aromatic hydrocarbons (PAHS) are $1/1000^{th}$ the width of a human hair and can linger in the air for up to two weeks. UFPs and

PAHs are capable of traveling long distances as well as penetrating filtration and conditioning units in buildings and cars. Additionally, they have the capacity to breach soft body tissues and enter bloodstreams, something larger particulates cannot achieve (Mohamad P. Zakaria, 2018).

Hydrocarbons (HC) can be referred to as volatile organic compounds (VOCs) and are hazardous air pollutants. The combination of carbon monoxide and hydrocarbon particulates produced by incomplete combustion contribute to contrails that form climate impacting cirrus clouds. Carbon monoxide emissions are produced from incomplete combustion of the carbon in fuel and are particularly harmful to humans.

In this study, carbon monoxide (CO), carbon dioxide (CO_2), water vapor (H_2O), nitrous oxides (NO_x), and total hydrocarbon (THC) emissions will be analyzed.

2.3 Noise, Vibrations and Harshness (NVH)

Pressure variations travel through any elastic medium from a sound source to a listener's ear (Measuring Sound, 1984). The number of pressure variations per second is the frequency of the sounds and is measured in Hz. The tone of a sound is produced by its frequency, with instances of thunder having low frequency and the sound of a whistle having a very high frequency. These two occasions of sound illustrate how low frequency pressure variations cause lower pitch sounds and high frequency pressure variations induce higher pitched sounds.

A pure tone is a sound that has only one frequency – a rare occurrence, as typically sounds are comprised of a variety of different frequencies (Measuring Sound, 1984). Broad band noise is the type of noise consisting of a mixture of frequencies and is encountered very often in noise analysis. The human ear is most responsive to sounds in the frequency

range of 500 Hz to 8,000 Hz but a broader range of frequencies will be analyzed in this study to understand the noise and vibrations of an operational aircraft turbine.

According to (Khardi, 2008), aircraft noise can vary in terms of frequency and level during a flight for three main reasons. To start, high frequency jet noise presents a 'zone of silence' in the axial downstream direction. In comparison, the emission of low frequency noise is maximized in the downstream direction. Due to the different sources of aircraft engine noise (consider the combustor, air frame, fan, compressor, etc.), each sound producer radiates noise in different directions. (Khardi, 2008) also considers how the different stages of flight cause varied sound patterns to be emitted. He notes that studying dominant frequencies emitted during aircraft operation is necessary to allow aircraft and engine developers to improve sound proofing of systems that could reduce overall noise emissions.

While the human perception of sound is very complex, (Khardi, 2008) explains that humans perceive broadband noise by dividing the frequency axis into bands, with third octave bands describing human hearing very effectively. (Khardi, 2008) states that broadband noise arises primarily from the combustion chamber during operation and from the turbulence in jet engines. Regarding broadband noise in the absence of dominant frequencies, the human ear identifies the central frequencies of all covered third-octave bands. In reference to cutting down general noise annoyances that humans perceive, it is important to recognize that human hearing is most sensitive to frequencies around 4 kHz. Other important frequencies that were observed in the study by (Khardi, 2008) include the 3.5 kHz characteristic fan noise section and the observed 1.142 kHz frequency band that potentially originated from the engine. At the higher frequency bands of 1 kHz – 7 kHz,

the turbine and compressor sections of jet engines emit tonal noise caused by flows over cavities and in the case of aircrafts, the air traveling over the landing gear and flaps during operation.

When discussing the frequencies of sound and vibrations, the term harmonics is used to describe the distortion of a sinusoidal waveform by waveforms of different frequencies (Simons, 2016). Any waveform, whatever the complexity of its shape, can be mathematically split into individual components called the fundamental frequency and various harmonic frequencies. In relation to the research gas turbine, the fundamental frequency refers to the rotation of the main shaft. Any harmonics discussed indicate the flaws of the component responsible for the fundamental frequency signal, and an order indicates a signal from a separate component. Harmonics can explain what is going on inside of the turbine and the resulting movements that are presented on the outside. Additionally, harmonics can indicate mechanical issues within the turbine such as worn bearings that cause imperfect rotation of the shaft around its axis. Frequency orders are frequency correlations to different mechanical components within the turbine, to include the compressor and turbine fins. For example, the gas turbine operating at 65,000 rpm will have a fundamental frequency of 1,083 Hz. If the compressor consists of 12 blades, a signal corresponding to the 12 blades will be present at ~13 kHz (12×1083 Hz = 12,996 Hz).

A triaxial accelerometer measures vibrations, movements in the form of oscillations, in three directions from the location on which it is placed. For this study, the three directional vibrational data is measured in $\frac{m}{s^2}$ over a specific time period. To allow for better readability the Fast Fourier Transform is employed to convert acceleration data from the time domain into the frequency domain. This transformation decomposes a sequence of

values into components of different frequencies, allowing for a better understanding of which frequencies produced the highest magnitude of acceleration. In order to compute the total movements of the system within a given time period into an understandable format, processing of the transformed directional vibrations is necessary. The governing equation for how to effectively process the directional data is given below.

$$Magnitude\ of\ Acceleration = \sqrt{a_x^2 + a_y^2 + a_z^2} \quad (3)$$

Equation 3 provides the vector sum or magnitude of the triaxial acceleration.

3 Methodology

3.1 Determination of Fuel Properties

In this study, a Parr 1342 constant volume calorimeter was used to measure the fuel's lower heating value (LHV). The average of multiple trials of both fuels were used to create the values in the Table 2 below.

Table 2. Fuel Properties Comparison IPK and Jet A

Properties	IPK	Jet A
Density (g/cm^3) @ 15 °C	0.762	0.806
Lower Heating Value (MJ/kg)	40.74	41.51
Dynamic Viscosity (cP) @ 40 °C	0.995	1.320
Ignition Delay (s)	5.31	3.26
Combustion Delay (s)	17.17	5.01
Derived Cetane Number	25.88	47.96

*Properties determined on site. Batch# 11POSF7629 for the synthetic kerosene.

Dynamic Viscosity

To measure the fuels' dynamic viscosity, a Brookfield DV II Pro rotational viscometer was used. While recording the viscosity of the fuels at 2°C increments from 26°C to 90°C, the spindle speed was maintained constant at 200 rpm. The viscosity,

measured in cp, was found to be 25% lower than Jet A when measured at 40°C, suggesting that IPK fuels atomize better than Jet A during spray. This difference can be seen in Figure 9 below.

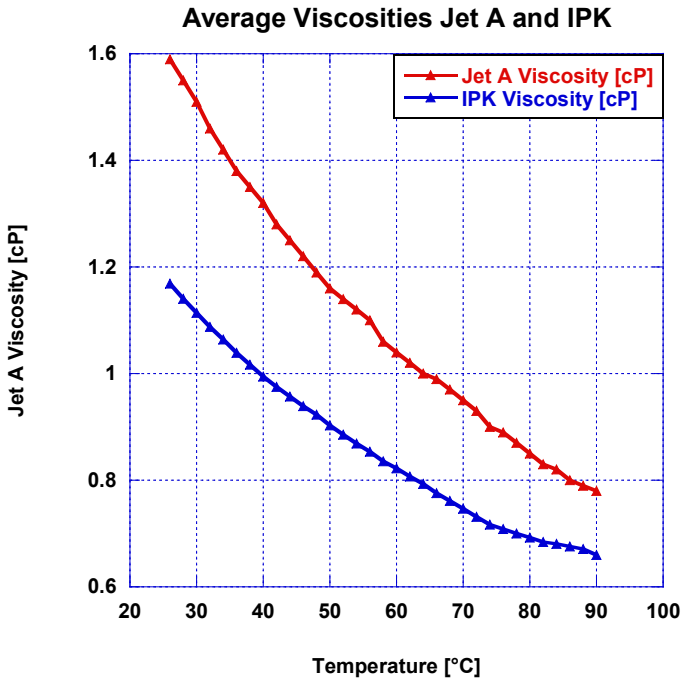

Figure 9. Dynamic Viscosity of IPK and Jet A

Lower Heating Value

To measure the fuel's lower heating value (LHV) a Parr 1341 constant volume calorimeter was employed. The LHV of Jet A obtained in the apparatus had an average value of 41.51 MJ/kg, compared to the LHV of IPK, which was measured at 40.7 MJ/kg.

TGA/DTA

A Shimadzu DTG-60 was utilized to conduct a thermogravimetric (TGA) and differential thermal (DTA) anlaysis of Jet-A and IPK for its vaporization rate and energy realease charecteristics. To maintain a control the experimental environment, the system was purged with low moisture compresed air at an airflow rate of 15 ml/min. The

temperature was increased incrementally from 20℃ at a rate of 20°C/min to a maximum temperature of 600℃. Using TGA, the change in mass for the fuel sample was measured and DTA measured the endothermic/exothermic energy levels for both fuels tested against a baseline.

The TGA for IPK and Jet A produced the numerical results found in Table 3 and the graphical results in Figure 10. From the tabulated data, TA10 corresponds to the temperatures at which 10% of each fuel mass was vaporized. The TA10 for IPK and Jet A were 70.5°C and 83.0°C, respectively. The lower temperature for IPK vaporization shows that IPK is more volatile than Jet A. Similarly, 50% of IPK's mass was vaporized at a temperature of 108.21°C compared to Jet A's TA50 of 130.12°C and 90% of IPK's mass was vaporized at a temperature of 132.2 °C, as opposed to Jet A's TA90 of 132.2°C. IPK's faster vaporization increases the mixing capabilities for a more uniform air/fuel mixture during combustion, increasing the combustion potential.

Table 3. TGA Results for IPK and Jet A

	Jet-A	**IPK**
TA10	83.0 °C	70.5°C
TA50	130.12°C	108.21°C
TA90	164°C	132.2°C

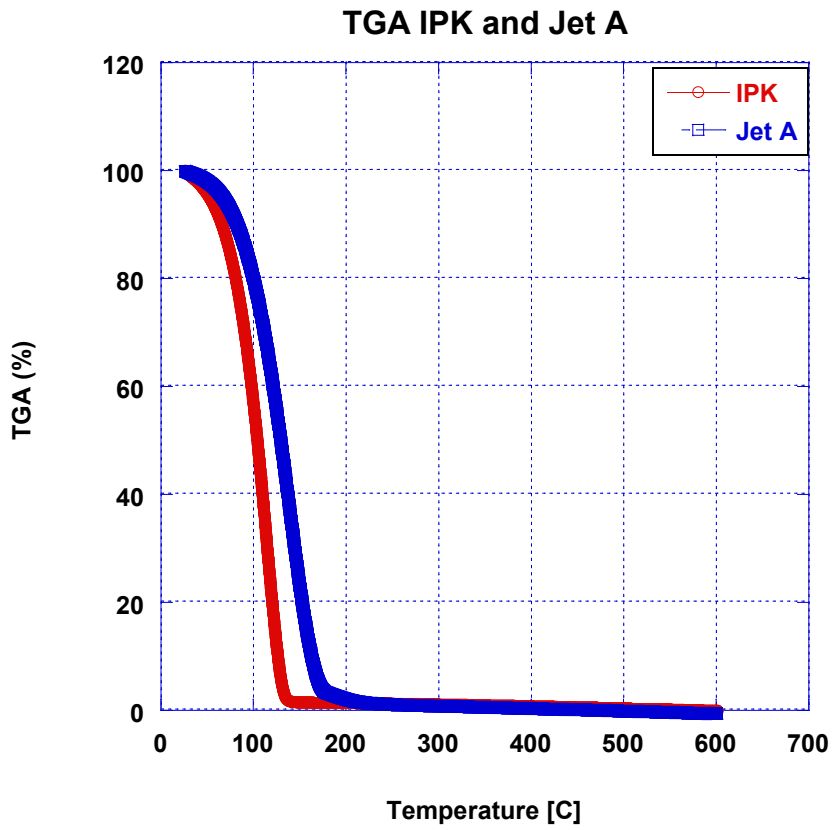

Figure 10. TGA analysis of Jet-A vs IPK

The purpose of the DTA of Jet A and IPK is to observe the low temperature heat release characteristics of both fuels. In the DTA graph below, the endothermic reaction of each fuel is defined as the concave down section of both curves. The exothermic reaction of the fuels corresponds to the concave up portions of the curves, where the curve is rapidly increasing. These results are in units of microvolts of energy per milligram of fuel. It is shown in Figure 11 below that IPK had a greater endothermic reaction than Jet A, as the minimum value of the curve occurs at a lower temperature of 124.6°C for IPK while Jet A's minimum value ocurs at 152.4°C. Additionally, IPK's peak at 160°C describes a greater exothermic reaction than that of Jet A, whose curve peaked at 200°C.

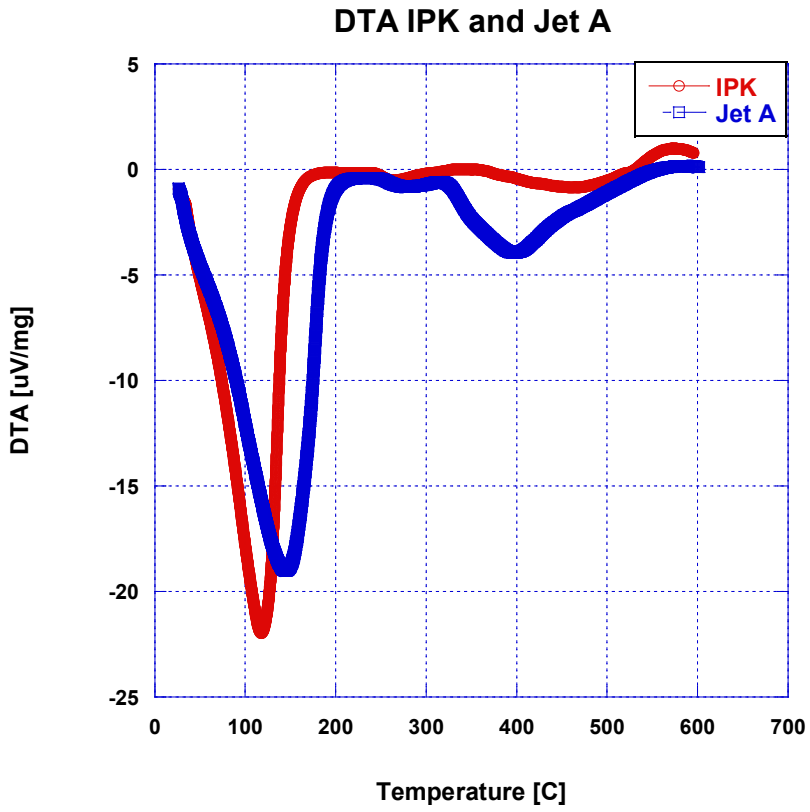

Figure 11. DTA analysis of Jet-A vs IPK

Spray Analysis with MIE Scattering He-Ne Laser

Using Mie scattering and Fraunhofer diffraction theories, a Malvern Spraytec He-Ne laser optical system was employed to analyze the atomization properties of Jet A and IPK. A single hole pintle type witness injector was utilized to inject fuel 100mm from the laser path. The data acquisition rate was 10 kHz and data was taken at standard atmospheric temperature and pressure with an injection pressure of 180 bar. Sampling lasted for 5 ms beginning 0.1 ms after the initial injection.

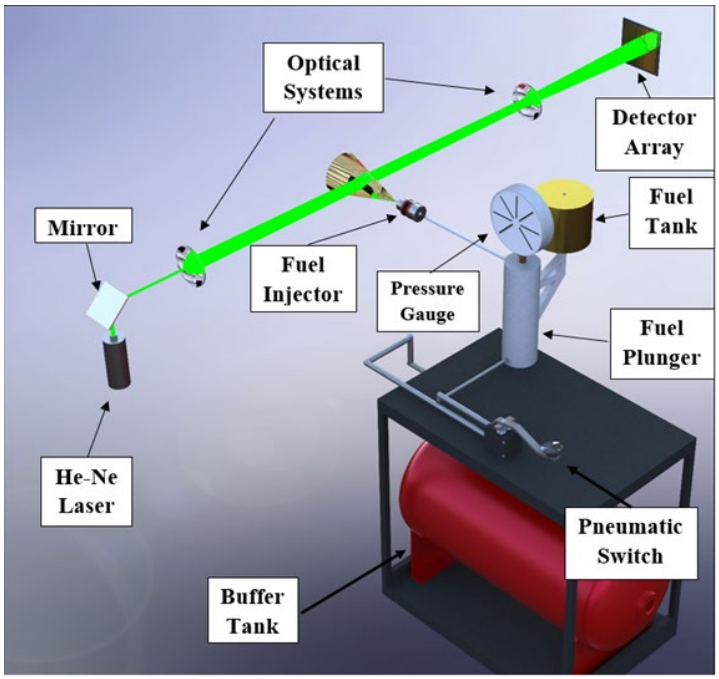

Figure 12. MIE Scattering Malvern Laser Experimental Configuration (Aerospace and Automotive Combustion Laboratory, Georgia Southern University)

Volume frequency data and Sauter Mean Diameter (SMD) measurements were taken for Jet A and IPK. The figure below describes the volume frequency and SMD as a function of time. Jet A showed a larger SMD than IPK over the spray time period. However, the spray volume frequency curves for Jet A and IPK followed the same general trend, with both curves reaching near the same peak volume frequency (%) value. It was found that IPK showed a higher spray volume frequency (%) at a lower SMD than Jet A, meaning that IPK vaporized faster than Jet A. This is also an indication of a lower viscosity and density for IPK.

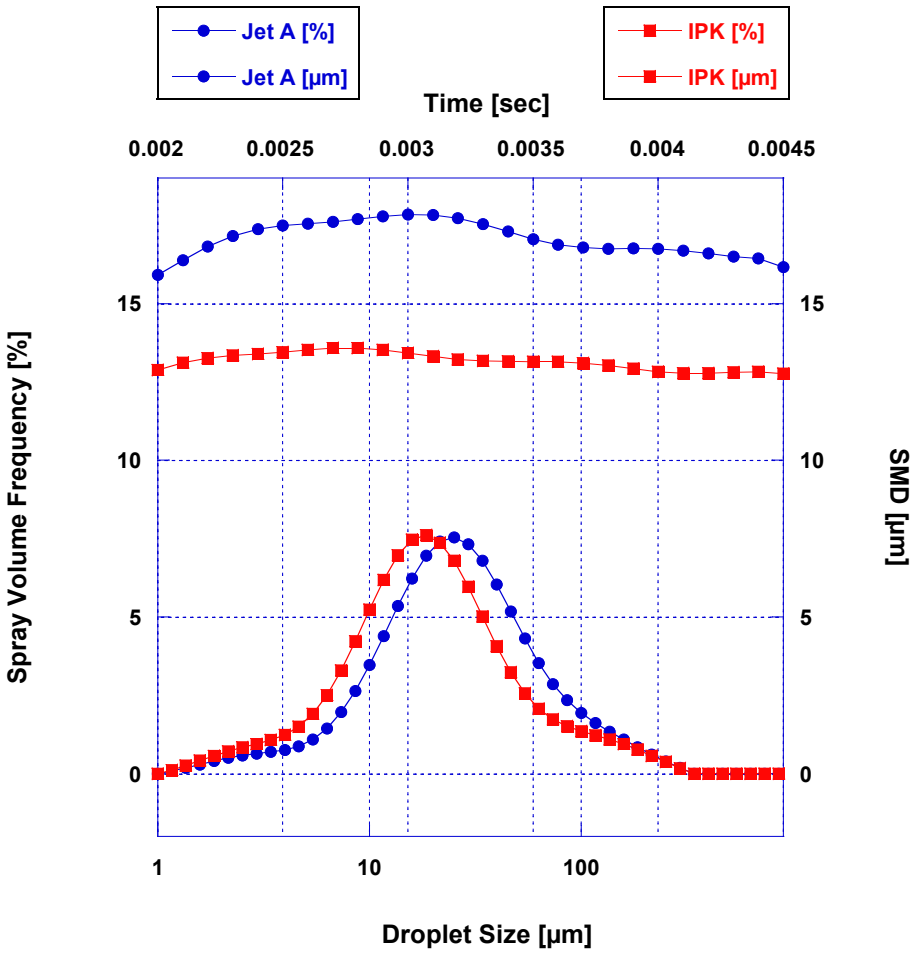

Figure 13. Spray Distribution of Jet A and IPK

Combustion Experimental Procedure

A PAC 510 constant volume combustion chamber (CVCC) was used to measure the combustion properties of neat IPK and Jet A under ASTM standard D7668-14a testing parameters for the measurement of the combustion properties of neat IPK and Jet-A. As displayed in Figure 14, the CVCC consisted of a 6 orifices Piezo Direct-Injector (1), a uniformly heated combustion chamber (2), a combustion pressure sensor (3), and Injection pressure sensor (4) (Soloiu, et al., 2020).

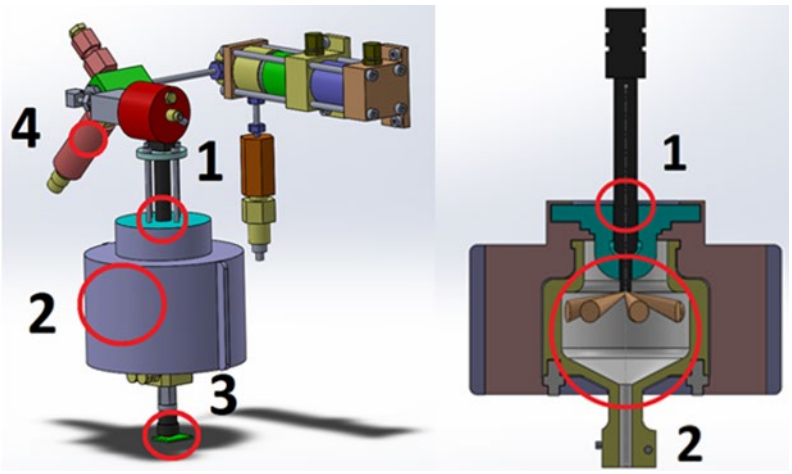

Figure 14. CVCC model (Aerospace and Automotive Combustion Laboratory, Georgia Southern University)

The CVCC testing parameters as described in ASTM standard D7668-14a are shown in Table 4, to include combustion chamber wall temperature, chamber pressure, injection pulse width, injection pressure, and coolant temperature. These parameters where held for all 15 combustion events per fuel with combustion pressure recorded for each event. The 15 combustion events pressure data was utilized in Equation 4 (Soloiu, et al., 2020) to determine the fuels Derived Cetane Number (DCN) with the use of Ignition delay (ID) and combustion duration (CD).

Table 4. ASTM Default Parameters in CVCC (Soloiu, et al., 2020)

ASTM Reference parameters:	
Combustion chamber Wall Temp.	595.5°C
Chamber pressure:	20 bar
Injection Pulse width:	2500 µs
Injection Pressure:	1000 bar
Coolant Temperature:	50°C

$$DCN = 13.028 + \left(\frac{-5.3378}{ID}\right) + \left(\frac{300.18}{CD}\right) + \left(\frac{-1267.90}{CD^2}\right) + \left(\frac{3415.32}{CD^3}\right) \quad (4)$$

The average pressure and Apparent Heat Release Rate (AHRR) for IPK and Jet A combustion are shown in Figure 15. With the ignition delay, combustion delay and derived cetane number displayed in Table 5, IPK is shown to be much less reactive than Jet A.

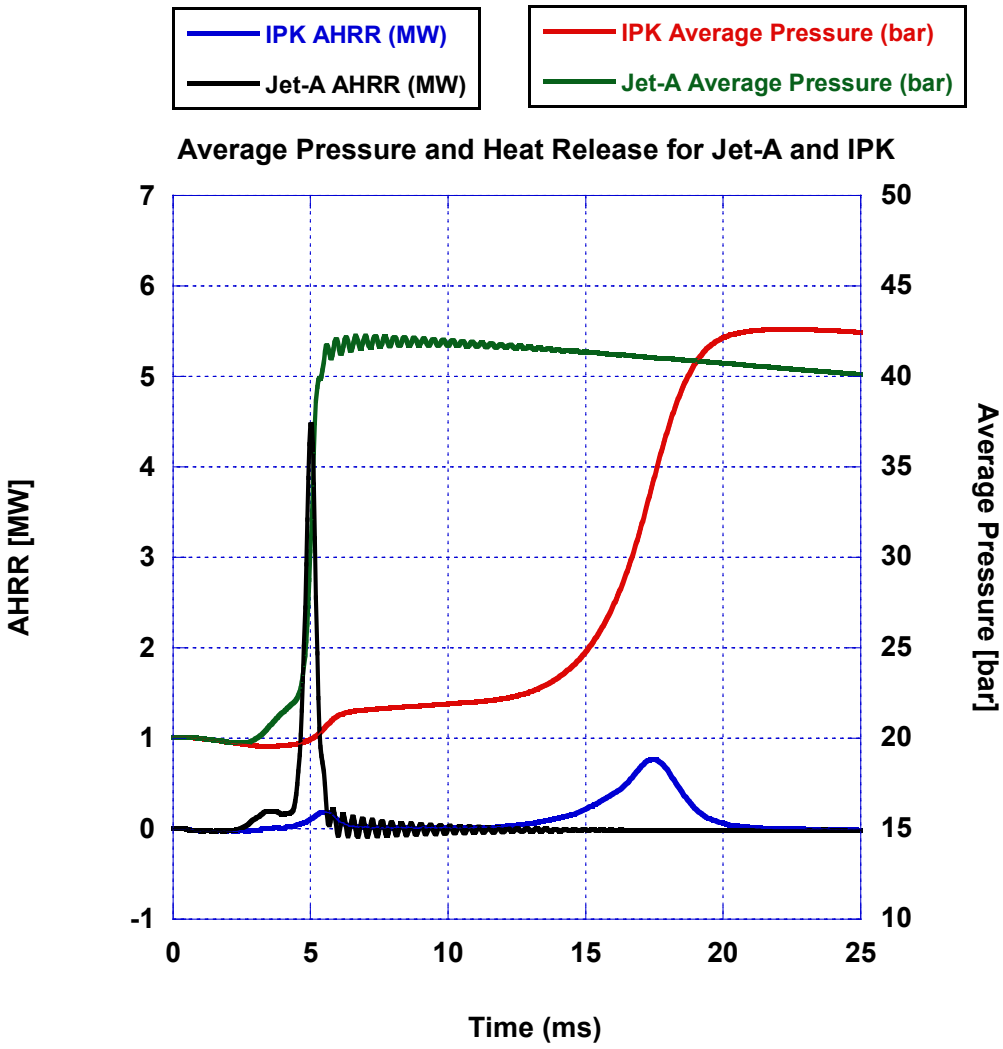

Figure 15. Pressure and Apparent Heat Release Rate for IPK and Jet A

Table 5. Combustion Properties for IPK and Jet A

Combustion Properties	IPK	Jet A
ID [s]	5.31	3.26
CD[s]	17.17	5.01
DCN	25.88	47.96

Because of IPK's extended combustion delay than Jet A, in Figure 15, IPK displays a lower initial AHHR peak as compared to Jet A's AHHR peak. Additionally, IPK has dual peaks as opposed to Jet A's only peak. IPK's two peaks are caused by the fuel's initial low temperature heat release that occurs around the 5 ms mark followed by the high temperature heat release that occurs at 17 ms.

3.2 Gas Turbine Experimental Set Up

An SR-30 experimental single stage gas turbine, pictured below, was used for testing. The gas turbine was instrumented with five pressure sensors (Setra Model 209) and K-type thermocouples at each stage of the turbine. The gas turbine included a flow meter for fuel flow and consumption as well as a FUTEK button type load cell sensor that can measure up to 100 lbs. With a maximum operating speed of 77,000 rpm, the gas turbine normal RPM speed range during experimentation was 60,000-70,000, with data acquisition performed at 65,000 rpm. Table 6 below describes the maximum operating conditions for the turbine.

Table 6. Turbine Maximum and Operating Conditions

(Minilab Gas Turbine Power System Operator's Manual, 2011)

	Maximum	Experimental
Max RPM	77,000	65,000
Max Inlet Temp (°C)	870	160
Max Exhaust Temp (°C)	720	489
Max Air Pressure (kPa)	1,103	999
Max Oil Pressure (kPa)	70	138
Max Ambient Temp (°C)	41	37

Additionally, the gas turbine had a maximum thrust of 40 lbf, a pressure ratio of 3.4 to 1, and a specific fuel consumption of 1.22 lb-fuel/lbf-hr. The engine has operational capabilities to run on a variety of fuel types to include Jet A, JP8, ULSD, biofuels, and synthetic fuels. The Data Acquisition board used was a National Instruments (NI6218) analog output.

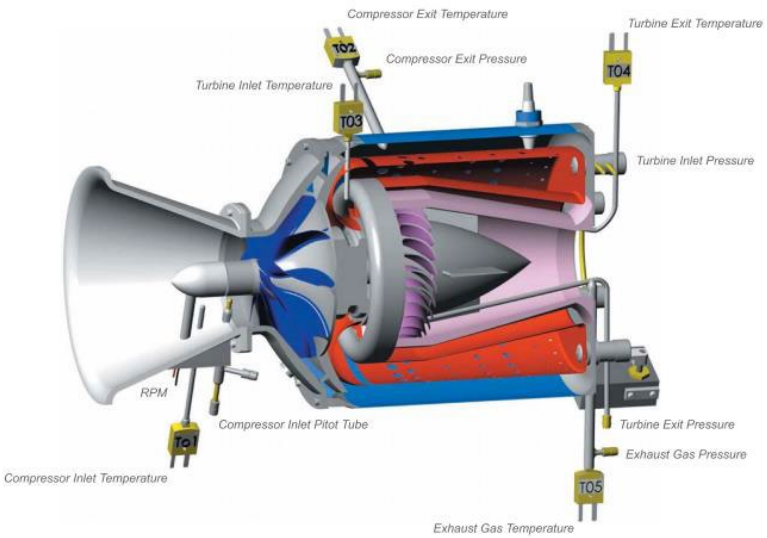

Figure 16. Cutout View of a Single Stage Jet Engine (C. Jensen, 2012)

3.3 Emissions Experimental Setup

An MKS Multigas FTIR Spectroscopy analyzer was employed to measure the ppm of 25 different species of gaseous byproducts in the exhaust fumes from the turbine. FTIR stands for Fourier transform infrared spectroscopy which is the process of passing infrared radiation through a sample. FTIR analysis measures the infrared wavelengths that are absorbed by a material which allows for the identification of gaseous emissions. The MKS MG200 software was used to continuously process the spectra while it computed the concentration of gases (MKS Instruments, 2016).

The MKS Gas Analyzer has specific temperature and humidity conditions under which it can be operated. These specifications are shown in Table 7 and Table 8 below.

Table 7. MKS Gas Analyzer Operating Temperatures and Allowable Variations (MKS Instruments, 2016)

	Operating Temperatures	Allowable Variation
Acceptable Operating Range	$10 - 32\ ^{o}C$ $(50 - 90\ ^{o}F)$ Some loss in signal to noise possible	$\pm 6\ ^{o}C$ $\pm 11\ ^{o}F$ Loss of signal to noise, baseline drift noticeable
Optimal Operating Range	$20 - 30\ ^{o}C$ $(68 - 86\ ^{o}F)$ Maximum performance range	$\pm 3\ ^{o}C$ $(\pm 5\ ^{o}F)$ No loss of performance, minimum baseline drift
Extreme Operating Range	$5 - 38\ ^{o}C$ $(40 - 100\ ^{o}F)$ Loss of signal to noise, electronics problems possible	

The exhaust temperatures of the turbine can reach temperatures surpassing 498 °C but the maximum temperature at which the gas can be analyzed in the MKS is 191 °C. This is because at any higher temperatures, the O-rings sampling line intake valve could melt

and the temperature constraints of the laser housings would be exceeded. To lower the temperatures of the exhaust gases so that they could be processed in the MKS through the sampling line, an exhaust gas transfer and heating pipe system was implemented. This piping system apparatus had multiple loops and allowed for the adequate cooling to an acceptable temperature for intake into the MKS.

Table 8. **MKS Gas Analyzer Optimal and Extreme Humidity Levels (MKS Instruments 2016)**

	Humidity Levels
Optimal Operating Range	$40\% - 60\%$
Extreme Operating Range	$10\% - 80\%$

According to the MKS Type Multigas™ Analyzer Models 2030, 2031 and 2032 Product Manual, the instrument was operated in a non-condensing environment and a dry nitrogen purge was run continuously for best performance. The acceptable humidity range for the MKS under a dry nitrogen purge is 10% - 90%. This range was narrowed to 40% - 60% humidity for optimal operating range with an extreme operational humidity level of 80% based on prior experimental results from runs of the MKS.

To promote the accuracy of the MKS during experimentation, certain days were chosen to experiment based on weather conditions to meet the MKS temperature and humidity specifications of the MKS. All tests were performed between the hours of 12 PM and 6 PM because, on average, the humidity levels in the afternoon are statistically lower than morning humidity levels.

3.4 NVH Experimental Setup

To minimize sound reflective surfaces, the turbine was moved to an open test bay for experimentation. Using the pressure sensors, thermocouples, and fuel flow rate

transmitters at the inlet and outlet, a National Instruments analog output model NI6218 collected pressure, temperature and flow data and displays it in a live graph while the speed (rpm) and thrust were also measured. The NI6218 transmitted and displayed the live readings to minilab software located on a designated turbine engine laptop.

Two Bruel & Kjaer (B&K) microphones were used to measure the mid to low range frequencies at the intake and exhaust nozzles as well as at the combustion chamber. A Prepolarized Free-field ½" Microphone Type 4966 was placed 1 m away from the turbine outlet (exhaust) at an angle of 45°. A Multi-field ¼" Microphone Type 4961 was placed 1 m away from the main body of the turbine, at an angle perpendicular from the main body. The specifications of the microphones are listed in Tables 9 and 10.

Table 9. Free-field 1/2" Microphone Type 4966 Specifications

Temperature	23 C
Ambient Static Pressure	101.3 kpa
Relative Humidity	50 %
Frequency	251.2 Hz
Polarization Voltage, external	0 V
Combined Sensitivity	-27.2 db re 1 V/Pa
Uncertainty 95% confidence level	0.2 db

Table 10. Multi-field 1/4" Microphone Type 4961 Specifications

Temperature	23 C
Ambient Static Pressure	101.3 kpa
Relative Humidity	50 %
Frequency	251.2 Hz
Polarization Voltage, external	0 V
Combined Sensitivity	-24.5 db re 1 V/Pa
Uncertainty 95% confidence level	0.3 db

Both microphones were mounted on tripods at a height level to that of the turbine midsection. A schematic for the orientation of the microphones can be seen in Figure 17 below.

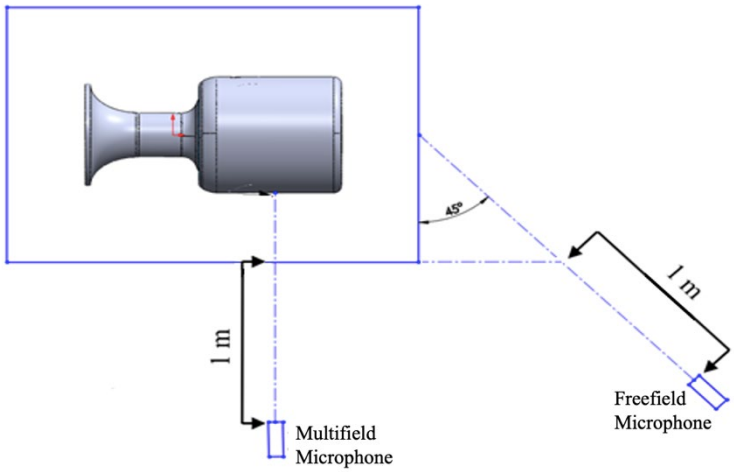

Figure 17. Microphone Experimental Setup Schematic

A Triaxial Deltatron Accelerometer Type 4527 was used to measure movement of the turbine in three directions during the experiments. The accelerometer specifications are shown in Tables 11 and 12.

Table 11. Triaxial Accelerometer Environmental Specifications

Environmental Temperature Range	-60º C to + 180ºc (-76ºf to +356ºf)
Temperature Coefficient of Sensitivity	+0.12%/ºc
Temp. Transient Sensitivity	0.02 ms^{-2}/ºc
Magnetic Sensitivity	15 ms^{-2}/T
Base Strain Sensitivity	0.1 ms^{-2}/µ€
Max. Non-destructive shock	50 kms^{-2} peak (5100 g peak)

Table 12.Triaxial Accelerometer Directional Specifications

	X	Y	Z
Reference Sensitivity	9.452 mv/g	9.939 mv/g	9.452 mvg
Frequency Range (Hz) : Amplitude (±10%)	0.3-10k[a] 0.3-5.5k[b]	0.3-10k[a] 0.3-5.5k[b]	0.3-12.8k[8]
Frequency Range (Hz): Phase (±5°)	2-10k[a] 2-5.5k[b]	2-10k[a] 2-5.5k[b]	2-12.8k[8]
Mounted Resonance Frequency (khz)	30[a] 19[b]	30[a] 17[b]	42[a]

As seen in Figure 18, B&K triaxial accelerometer was positioned on the turbine support plate to measure axial vibrations during combustion. Turbine axis orientations were assigned as shown in Figure 19, with the X-axis as the parallel to the turbine, Y-axis as perpendicular to the turbine, and Z-axis as the radial direction.

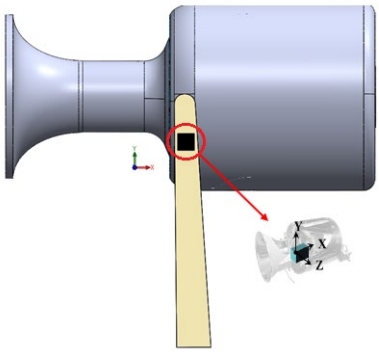

Figure 18. Triaxial Accelerometer Experimental Placement (Kilpatrick, 2019)

Figure 19. Turbine Axis Orientation Schematic

3.5 Experimental Setup Assembly and Processing

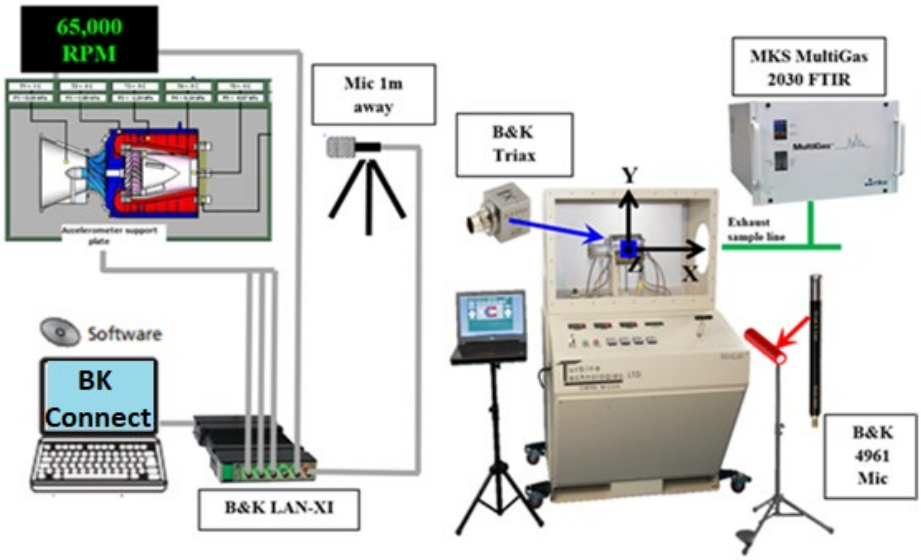

Figure 20. Experimental Engine and Noise, Vibrations, and Emissions Instrumentation (Simons, 2016)

For this experiment, sound pressure and acceleration measurements were taken at 65,000 RPM for Jet A and IPK. Gaseous emissions measurements were also taken for Jet A and IPK comparison. BK Connect software was applied to obtain and post process the vibrations and noise data from the turbine fuel testing. Constant Percentage Bandwidth (CPB) and Fast Fourier Transformation (FFT) analysis within this software was employed to evaluate the data. The emissions data was post processed using the MKS MG2000 software within the Multigas FTIR Spectrometer and the data produced was then analyzed.

Using the rpm sensor at the inlet of the turbine, the shaft speed was acquired. Temperature and pressure measurements were taken at the previously mentioned sensor locations on the turbine to include the areas of the compressor inlet, turbine inlet, turbine exit and exhaust. Sound pressure measurements were taken at a distance of 1m from the turbine combustion and 1m at a 45-degree angle from the turbine exhaust. The accelerometer was mounted on the turbine support plate which allowed for acceleration measurements to be taken as well. During operation these measurements were taken through the use of the measurement chain process below.

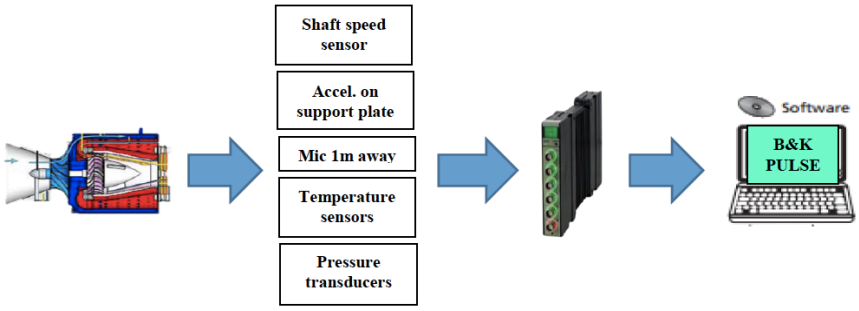

Figure 21. Measurement chain and DAQ Processes

The CPB analysis employed on the sound pressure measurements is a common way to analyze sound levels by separating the signals into the basic frequency constituents. The Fast Fourier Transform analysis method for the acceleration (vibration) measurements allowed for the conversion from the time domain to a representation in the frequency domain, similar to CPB. Both the FFT and CPB analysis utilize Euler's equations for complex transformations. The bandwidth organization was based on 1/3 octave bandwidths and A weighting, as A weighting focuses on the human hearing capabilities.

The frequency range considered for the sound pressure was the range of 0 kHz to 16 kHz and for acceleration, the range was set at 0 kHz to 25.6 kHz. This was chosen in order to examine the gas turbine's behavior on a broad frequency range and identify the

frequencies of key mechanical components within the turbine. All Fourier analysis was judged on the differences in decibels, specifically differences of 3 decibels or more, as humans are able to notice changes in sound at this difference level.

4 Results and Discussion

The following data include results from a total of four turbine runs: three runs of IPK and one run of Jet A, all at 65,000 rpm operating speed. The results were averaged for the three turbine experiments with IPK and compared to the Jet A results. This low number of experiments performed for the Jet A fuel was due to the university shut down as a result of COVID-19 and the lack of specific weather conditions required to operate the turbine and the emissions analyzer.

4.1 NVH Results

First, the noise, vibrations, and emissions data of Jet A and IPK at an operating speed of 65k RPM were recorded and processed to produce the results seen below. The frequency range for the IPK and Jet A sound pressure data set was 16 kHz and the sound pressure measurements were processed with a CPB. Only the free field sound pressure measurements were analyzed in this study. The free field microphone was placed at 45 degrees to the exhaust of the turbine while it was running. The frequency range for the triaxial acceleration data was set to 25.4 kHz. The free field sound pressure measurements for IPK and Jet A at 65,000 rpm are shown in Figure 18 below.

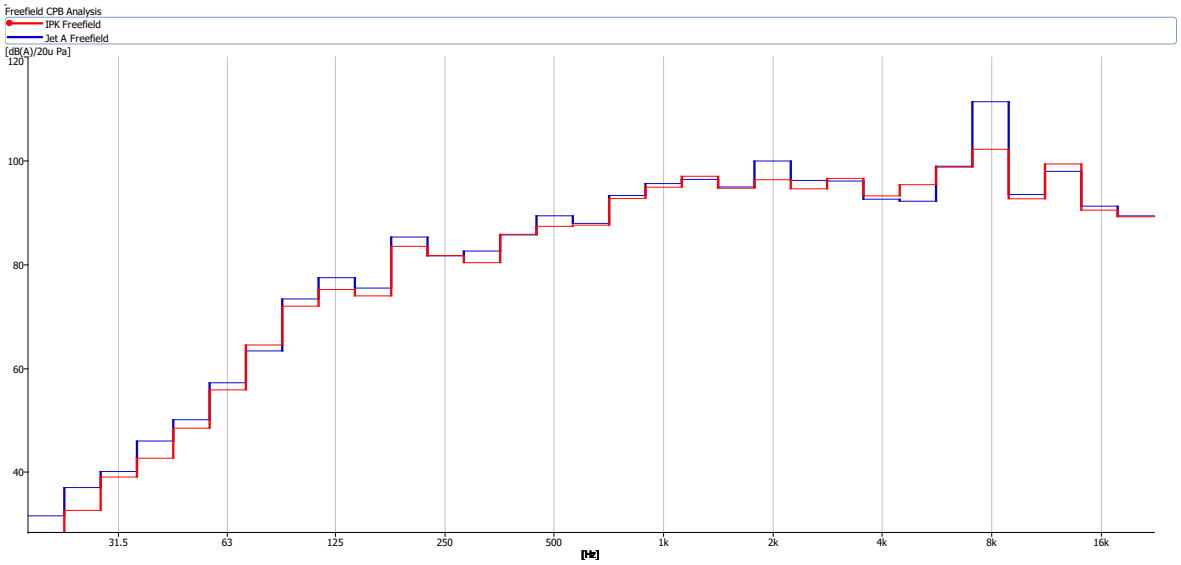

Figure 22. IPK and Jet A Comparative Free Field Sound Pressure Measurements at 65k rpm operating speed

The 1-8kHz range is considered to be the upper frequency range (high pitched) and would be considered very loud and uncomfortable to the human ear. The two fuels follow the same general trend, with the greatest variation in sound pressure profile occurring at the 2 kHz and 8 kHz frequency locations. At the 2 kHz location, Jet A showed slightly higher sound pressure measurements than IPK, producing 100 db(A)/20 u Pa compared to IPK's 95 db(A)/20 u Pa. At the 8 kHz frequency location, Jet A reached an extreme free field sound pressure level of 112 db(A)/20 u Pa while IPK produced 102 db(A)/20 u Pa. However, taking into account that human hearing is most sensitive to frequencies around 4 kHz, IPK could be perceived by humans as causing more noise. Figure 22 indicates that the sound signatures for each fuel generally resemble each other across the frequency span.

The triaxial vibration measurements for each trial were first processed using FFT, then the vector sum of the three directional accelerations was obtained. The vector sum of acceleration from the trial were averaged to display an overall acceleration measurement.

The overall spectrum for each set of vibration measurements clearly indicates orders that were excited the most.

The locations of primary concern for the vibration data set are as follows: around 1.083 kHz, which correlated to shaft rotation (65,000 rpm = 1,083 Hz), the third order at 3.2kHz, matching up to the three turbine exit fins (three fins, 3 × 1,083 Hz = 3,249 Hz), and the twelfth order at ~13 kHz, corresponding to the compressor blades (twelve blades, 12 × 1,083 Hz = 12,996 Hz). For each RPM, the corresponding operating frequency and additional frequencies for consideration are shown in Table 13.

Table 13. Mechanical Properties of the Aero-Gas Turbine and Corresponding Frequencies

RPM	**65,000**
Operating Frequency – Shaft Rotation	1,083 Hz
3 Fins	3,249 Hz
12 Compressor Blades	12,996 Hz

In Figure 23 below, the overall acceleration profile comparison of Jet A and IPK is shown.

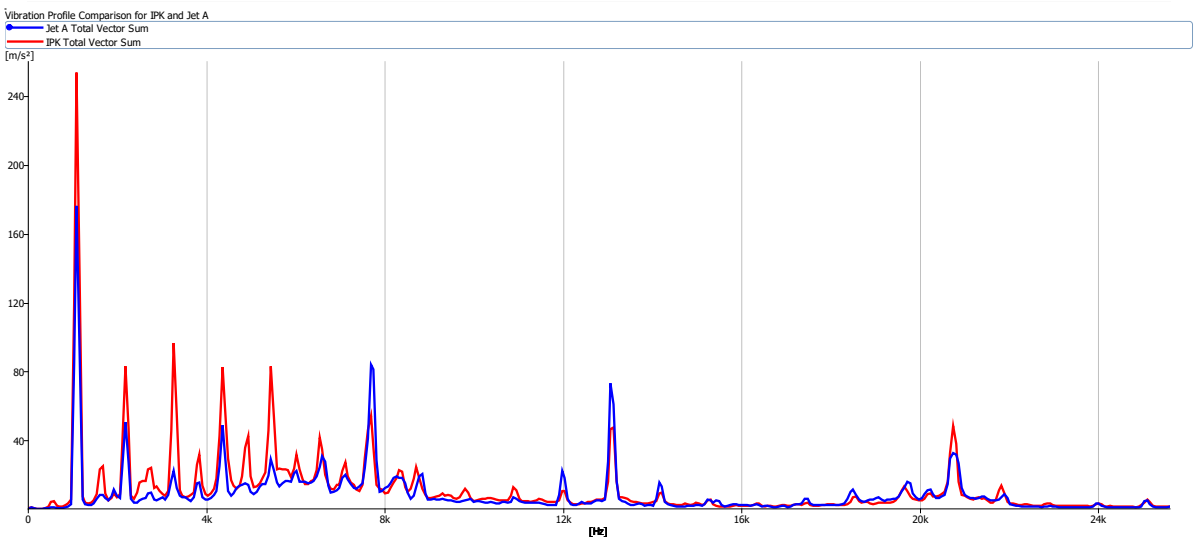

Figure 23. Full Jet A and IPK Vibration Profile Comparison at 65k rpm operating speed

Across the lower frequencies (0-8kHz) it is obvious that IPK has a higher general amplitude of acceleration than Jet A. There are a few cases of Jet A showing higher vibration levels at peak locations such as just before the 8kHz region and around the 13 kHz region, but other than those, IPK shows more vibrational disturbance overall. For a better understanding of specific regions of interest, Figures 24 and 25 below show magnified sections of frequency ranges 0-8kHz and 8 - 24 kHz.

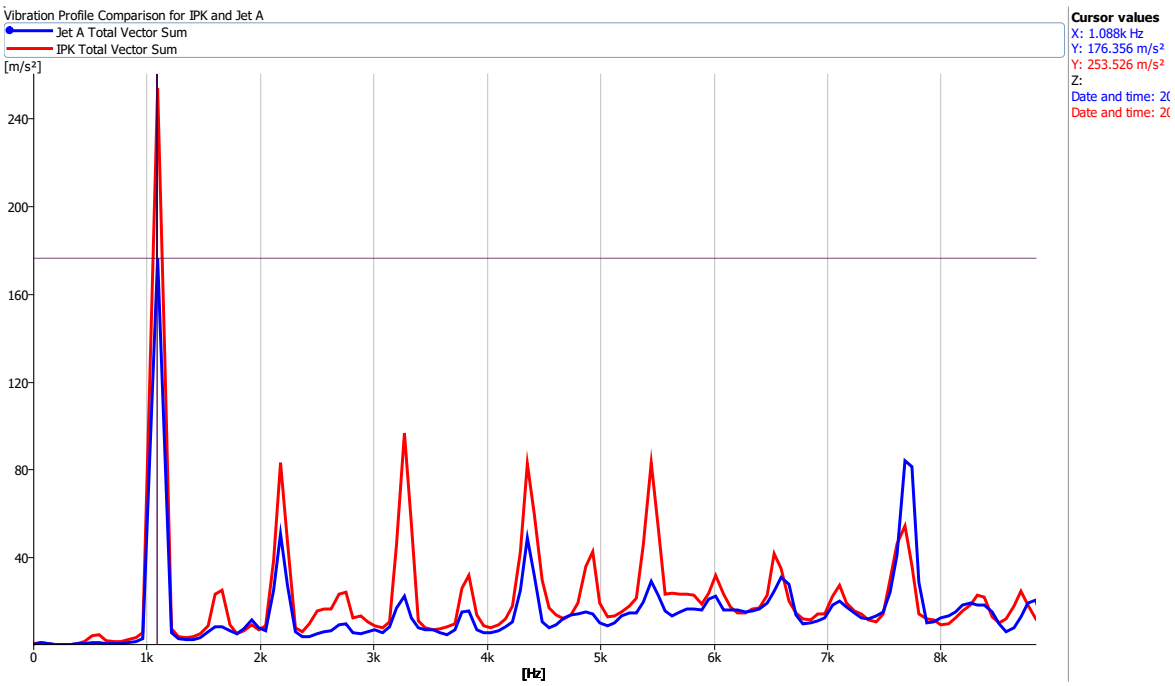

Figure 24. Zoom Jet A and IPK Vibration Profile Comparison at 65k rpm operating speed for frequency range 0-8kHz

At the 1 kHz frequency location (shaft rotation), IPK reaches a maximum acceleration of 253.526 m/s^2, with Jet A showing significantly lower acceleration of 176.356 m/s^2. Around the 3.2kHz frequency location (three turbine exit fins), IPK reads 96.84 m/s^2 acceleration with Jet A only displaying 22.58 m/s^2 acceleration. This substantially higher amplitude of vibration at the shaft rotation in IPK profile as compared to Jet A is most likely due to the low temperature heat release that IPK displays during combustion. IPK has a higher ignition delay and combustion delay which produces a more unstable combustion reaction. Additionally, this causes IPK to have a greater endothermic and exothermic reactions in comparison to Jet A and results in higher amplitudes of combustion vibrations in the shaft and three turbine exit fins when IPK is employed.

Aside from the specific frequency locations of interest in the 0-8kHz frequency range, IPK also has greater levels of acceleration in each of the normal short vibrational

peaks that are seen between 1 kHz and 8 kHz. Although the disparity is less than what is seen at the specific 1 kHz and 3.2 kHz areas mentioned previously, it is important to note that the more powerful combustion reactions of IPK have vibrational effects that are greater than that of Jet A. Figure 25 below illustrates the IPK and Jet A vibrational profile comparison at 65,000 rpm between the frequencies of 8 kHz and 24 kHz.

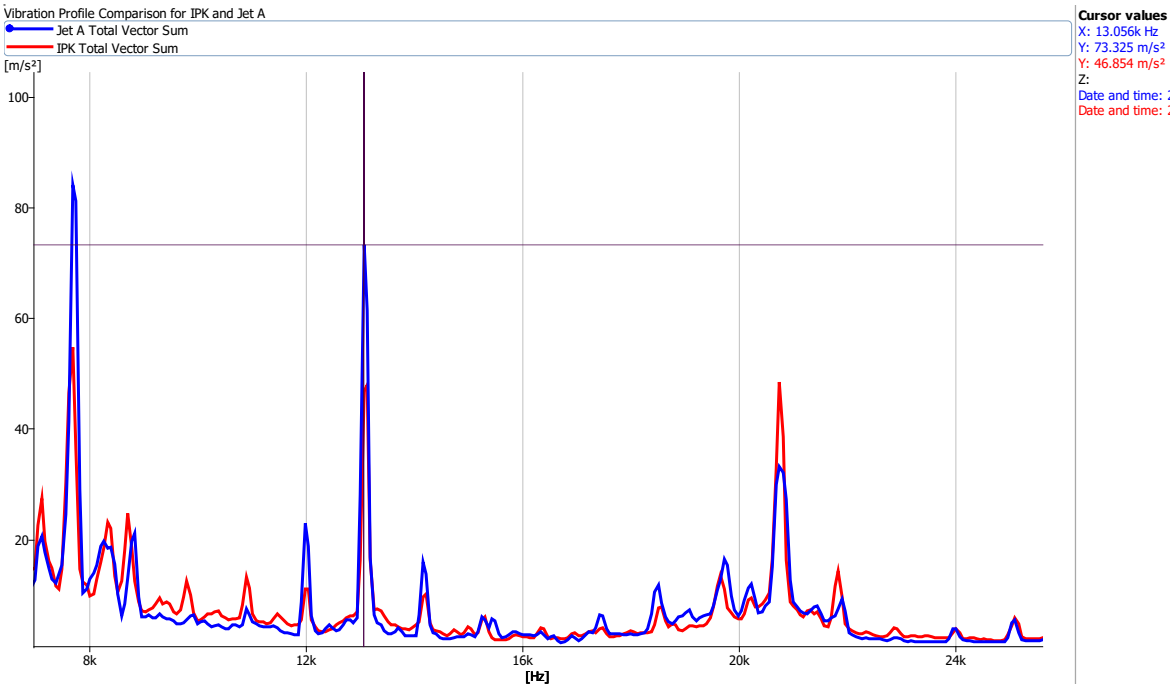

Figure 25. Zoom Jet A and IPK Vibration Profile Comparison at 65k rpm operating speed for frequency range 8-24kHz

From Figure 25 in the 8-24 kHz frequency range, the fuels follow the same general trend. In this range, it can be seen that while the vibration measurements are much less disparate than in the lower frequency range, Jet A actually shows higher acceleration than IPK at most of the peaks. Around the 8 kHz region, Jet A reaches an extreme value of 83.493 m/s^2 with IPK showing a reading of 55.076 m/s^2. The spike in the 8 kHz region could mean significant mechanical movement in the ball bearings of the turbine in the radial direction. At the 13 kHz region (12 compressor blades), Jet A again expresses a higher acceleration of 73.325 m/s^2 while IPK displays 46.854 m/s^2 acceleration. Reasoning

for why Jet A has higher vibrational patterns than IPK at higher frequencies is unknown at this time.

4.2 Gaseous Emissions

The emissions of Jet A and IPK were measured at the exhaust and analyzed using a Multigas 2030 FTIR Spectrometer. The results of this analysis are shown in Table 14 below. As an alternative fuel, IPK is derived from coal using the Fischer-Tropsch process and known for having little to no aromatics, making it, in theory, a fuel that is less detrimental to the atmosphere as far as its emission of greenhouse gasses. These specific exhaust gases were chosen as the most crucial to monitor and mitigate in jet fuel exhaust.

Figures 26 and 27 below illustrate the gaseous emissions results from using Jet A and IPK fuels in the experimental turbine at an operating speed of 65k rpm. Table 14 numerically summarizes the data shown in the figures. The measurements are shown in percentage of total gas exhaust volume as well as in parts per million by volume.

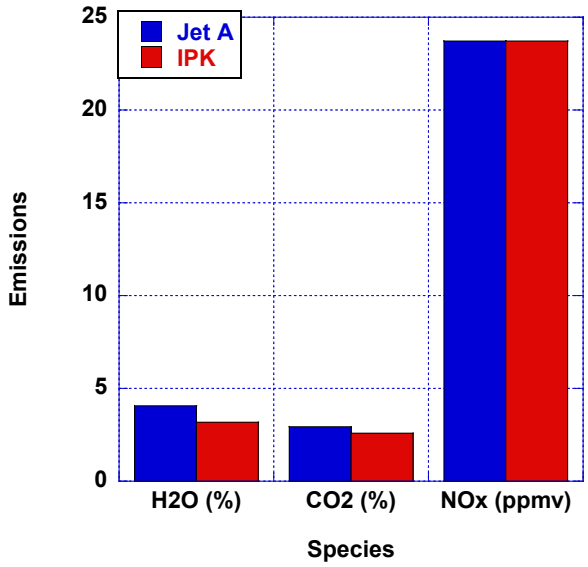

Figure 26. Average Jet A and IPK H20, CO2, and NOx Gaseous Emissions at 65k RPM

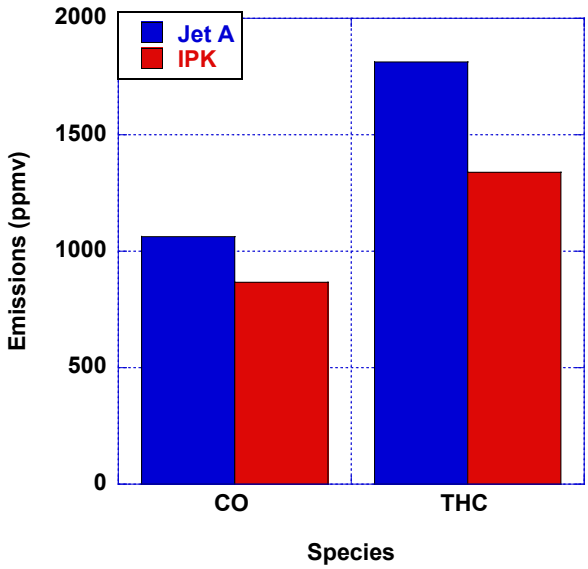

Figure 27. Average Jet A and IPK CO and THC Gaseous Emissions (ppmv) at 65k RPM

Table 14. Average Jet A and Gaseous Emissions Results at 65k RPM

Species	Jet A	IPK	% Difference between Jet A and IPK
H_2O (%)	4.059	3.186	- 24.0994%
CO_2 (%)	2.947	2.586	- 13.049%
NO_x (ppmv)	23.722	23.713	- 0.0379467%
CO (ppmv)	1062.892	867.466	- 20.2476%
THC (ppmv)	1812.247	1338.701	- 30.0574%

* Are shown as % of exhaust gas sampled

As observed in Table 14, IPK provided a reduction in every emissions species in comparison to Jet A. While NO_x emissions were reduced by less than 1%, all the other areas of IPK gaseous emissions showing significantly lower levels than Jet A, with a minimum difference of 10% across the board.

5 Conclusions

In comparison to Jet A, IPK was found to have a lower heating value, a lower dynamic viscosity, a shorter ignition and combustion delay, a lower derived cetane number, a smaller SMD, and a larger spray volume distribution. IPK had lower thermal stability during the heat release stage of combustion, with a greater exothermic and endothermic reaction occurring. These qualities impacted the combustion of IPK within the turbine, causing significantly higher vibrations in the shaft rotation and turbine exit fins. It was found that in the lower frequencies of vibrations (0 kHz – 8 kHz) within the turbine, IPK produced higher amplitudes of vibration. At the higher frequency range (8 kHz – 24 kHz), Jet A produced slightly higher levels of vibrations. While there was some variation in peak vibrational amplitudes of the two fuels, there were almost no disparities between the sound

pressure levels of the two fuel runs at the turbine exhaust, with the sound profiles of the fuels closely resembling each other. In reference to the emissions analysis, IPK performed better than Jet A, as it produced significantly less gaseous emissions (in ppmv and % of volume) in every species analyzed.

In the future, NVH and emissions testing of different ratios of fuel blends would be beneficial, to include Jet A, IPK, and S8. Repeat testing of the fuels will be necessary in order to provide accurate data. Potential future work includes noise vibrations and harshness testing at higher frequencies 25 kHz + to analyze the 26 turbine blades functionality within the turbine. At an rpm of 65,000, the turbine blades corresponding frequency would be 70.395 kHz (operating frequency of $1{,}083\,Hz \times 26\,turbine\,blades = 70{,}395\,Hz$). Conversely, this testing could be performed at lower rpms so that the corresponding frequency of the 26 turbine blades would be significantly lower. For example, if the turbine were operated at 45,000 rpm, the operating frequency would correspond to 750 Hz, allowing the 26 turbine blade frequency to occur at 19,500 Hz instead of 70396 Hz. Additionally, noise vibrations and harshness testing as well as emissions analysis could be performed while accelerating or decelerating the turbine to provide data on theoretical take-off and landing situations for aircrafts. Finally, a broader range of gaseous emissions should be analyzed for a deeper understanding of the gaseous emissions qualities of Jet A and IPK.

6 References

This research was supported by DoD-NSF Assure REU Site Award: 1950207 and experimental fuel contributions from the Air Force Research Laboratory.

Atif Qasim MD, M. (n.d.). *Wave Parameters*. Retrieved 9 28, 2020, from https://www.echocardiographer.org/Echo%20Physics/Wave%20parameters.html

(2005). *Aviation & Emissions A Primer.* Federal Aviation Administration Office of Environment and Energy.

Balachandar Gopalakrishnan, N. K. (2019). Chapter 4: Dark-Fermentative Biohydrogen Production. In *Biohydrogen* (pp. 79-122). Elsevier.

Brandon Graver, P., Zhang, K., & Dan Rutherford, P. (2018). CO2 emissions from commercial aviation (working paper). *Working Paper 2019-16, The International Council on Clean Transportation*.

C. Jensen, H. L. (2012). *Modeling and Validation of the SR-30 Turbojet Engine*. Retrieved October 26, 2019

Chi Zhang, X. H.-J. (2014). "Recent development in studies of alternative jet fuel combustion: Progress, challenges, and opportunities.". *Renewable and Sustainable Energy Reviews 126*.

David Carbaugh, M. C. (n.d.). *In-Flight Airplane Vibration and Flight Crew Response*. Retrieved 2019, from http://www.boeing.com/commercial/aeromagazine/aero_16/vibration_story.html.

ENGINEERS, I. O. (2020). *Engineering Code of Ethics*. Retrieved October 1, 2020, from https://www.iise.org/details.aspx?id=299#:~:text=The%20Fundamental%20Canons&text=Engineers%20shall%20hold%20paramount%20the,performance%20of%20their%20professional%20duties.&text=Engineers%20shall%20act%20in%20professional,shall%20avoid%20conflicts%20of%2

EPA. (2016, August 2). *Climate Change Indicators: Oceans*. Retrieved from https://www.epa.gov/climate-indicators/oceans

Fleming, S. (2009). *Aviation and Climate Change: Aircraft Emissions Expected to Grow, but Technological and Operational Improvements and Government Policies Can Help Control Emissions.* Washington D.C.: United states Government Accountability Office.

Ghosh P., J. S. (2006). Detailed Composition-Based Model for Predicting the Cetane Number of Diesel Fuels. *Industrial & Engineering Chemistry Research*, 346-351.

J. Yanowitz, M. R. (2017). *Compendium of Experimental Cetane Numbers.* National Renewable Energy Laboratory.

James I. Hileman, D. S. (2009). *Near Term Feasibility of Alternative Jet Fuels.* Cambridge, MA: RAND Corporation and Massachusettes Institute of Technology.

(2005). *Jet Engine Basic Through Thrust Analysis.* Cleveland, Ohio: Ultra Efficient Engine Technology Office of NASA Glenn Research Center.

Julia Heimberger, M. M. (n.d.). Synthetic Aviation Fuels. Statesboro: Georgia Southern University.

Khardi, S. (2008). An Experimental Analysis of Frequency Emisison and Noise Diagnosis of Commercial Aircraft on Approach. *J. Acoustic Emission, 26*, 290-310.

Kilpatrick, M. (2019). The Investigation of Noise, Vibrations, and Emissions of Aero-Gas Turbine Combustion wiht Synthetic Kerosens. *Honors Undergraduate Thesis*. Statesboro: Georgia Southern University.

Klerk, A. d. (2000). Fischer - Tropsch Process. *Kirk - Othmer Encyclopedia of Chemical Technology*, pp. 1-20.

M Dost, R. J. (2016). *Fighting Noise in Gas Turbines.* Amsterdam, Netherlands: AviationFacts.eu.

Mathias Basner, M. P. (n.d.). *Aviation Noise Impacts: State of the Science.* Noise and Health.

Measuring Sound. (1984). Retrieved 9 4, 2020, from Bruel & Kjaer Sound & Vibration Measurement A/S: http://www.bksv.com/doc/br0047.pdf

Minilab Gas Turbine Power System Operator's Manual. (2011). In *Turbine Technology.* LTD.

MKS Instruments, I. (2016). MKS Type MultiGas™ Analyzer Models 2030, 2031 and 2032 Manual. Wilmington, MA .

Mofid Gorii-Bandpy, M. A. (2012). Airfram Noise Sources and Reduction Technologies in Aircraft. *Noise and Vibration Worldwide*, pp. 29-32.

Mohamad P. Zakaria, C.-W. B. (2018). Chapter 16 - Fingerprinting of Petroleum Hydrocarbons in Malaysia Using Environmental Forensic Techniques: A 20-Year Field Data Review. *Oil Spill Environmental Forensics Case Studies*, 345-372.

Moses, C. A. (2008). *Comparative Evaluation of Semi-Synthetic Jet Fuels.* Alpharetta, GA and Dayton, Ohio: U.S. Air Force Research Laboratories through Universal Technology Corporation.

Prem Lobo, J. C.-L. (2016). Demonstration of a Regulatory Method for Aircraft Engine Nonvolatile PM Emissions Measurements with Conventional and Isoparaffinic Kerosene fuels. *Energy Fuels*, 7770-7777.

Program, U. G. (n.d.). *Observed Change | National Climate Assessment*. Retrieved November 2, 2019, from https://nca2014.globalchange.gov/report/our-changing-climate/observed-change.

Program, U. G. (n.d.). *Observed Change | National Climate Assessment*. Retrieved November 2, 2019, from https://nca2014.globalchange.gov/report/our-changing-climate/observed-change.

R., C. R. (2012). Effect of Cetane Number on Specific Fuel Consumption and Particulate Matter and Unburned Hydrocarbon Emissions from Diesel Engines. *Journal of Combustion*.

Rao, S. S. (2010). Fundamentals of Vibration. In S. S. Rao, *Mechanical Vibrations (5th Edition)* (pp. 1-120). Pearson.

Richard Striebich, L. S. (2008). *DEPENDENCE OF FUEL PROPERTIES DURING BLENDING OF ISO-PARAFFINIC KEROSENE AND PETROLEUM-DERIVED JET FUEL .* WRIGHT-PATTERSON AIR FORCE BASE, OH: University of Dayton Research Institute.

Robert J. Santoro, T. A. (2007, September 17). Generation of Comprehensive Surrogate Models and Validation Databases for Simulating Large Molecular Weight Hydrocarbon Fuels. Princeton, NJ.

Sadeghbeigi, R. (2012). Chapter 3 - FCC Feed Characterization. In *Fluid Catalytic Cracking Handbook (Third Edition)* (pp. 51-86). Butterworth-Heinemann.

Simons, E. (2016). *Electronic Theses and Dissertations.* Retrieved 6 20, 2020, from Investigations of the Combustion Sound and Vibration Characteristics of an Aero-derivative Gas Turbine: https://digitalcommons.georgiasouthern.edu/etd/1516

Soloiu, V., Wiley, J. T., Gaubert, R., Mothershed, D., Carapia, C., Smith, R. C., . . . Rahman, M. (2020). Fischer-Tropsch coal-to-liquid fuel negative temperature coefficient region (NTC) and low-temperature heat release (LTHR) in a constant volume combustion chamber (CVCC). *Energy*, https://doi.org/10.1016/j.energy 117-288.

Swift, H. (2010). *A Review of Literature Related to Potential Health Effects of Aircraft Noise.* West Lafayette, Indiana: U.S. Federal Aviation Administration Office of Environment.

Sylvester Abanteriba, U. Y. (2016). Derived Cetane Number, Distillation and Ignition Delay Properties of Diesel and Jet Fuels Containing Blended Synthetic Paraffinic Mixtures. *SAE International Journal of Fuels and Lubricants*, 703-711.

Tara J Fortin, A. L. (2015). Viscosity Measurements of Avition Turbine Fuels. *Energy and Fuels 12*.

Transporation, U. D. (2018). *Aircraft Noise Issues*. Retrieved October 29, 2019, from https://www.faa.gov/about/office_org/headquarters_offices/apl/noise_emissions/airport_aircraft_noise_issues/

University, P. (1998). *Noise Control*. Retrieved November 10, 2019, from https://engineering.purdue.edu/~propulsi/propulsion/jets/basics/noise.html.

Yi Yang, A. L. (2007). A study of jet fuel sooting tendency using the trheshold sooting index model. In *Combustion and Flame* (pp. 191-205). Elsevier.